Climatological Characterization of Three-Dimensional Storm Structure from Operational Radar and Rain Gauge Data

MATTHIAS STEINER, ROBERT A. HOUZE JR., AND SANDRA E. YUTER

Department of Atmospheric Sciences, University of Washington, Seattle, Washington

(Manuscript received 26 September 1994, in final form 1 March 1995)

ABSTRACT

Three algorithms extract information on precipitation type, structure, and amount from operational radar and rain gauge data. Tests on one month of data from one site show that the algorithms perform accurately and provide products that characterize the essential features of the precipitation climatology. Input to the algorithms are the operationally executed volume scans of a radar and the data from a surrounding rain gauge network. The algorithms separate the radar echoes into convective and stratiform regions, statistically summarize the vertical structure of the radar echoes, and determine precipitation rates and amounts on high spatial resolution.

The convective and stratiform regions are separated on the basis of the intensity and sharpness of the peaks of echo intensity. The peaks indicate the centers of the convective regions. Precipitation not identified as convective is stratiform. This method avoids the problem of underestimating the stratiform precipitation. The separation criteria are applied in exactly the same way throughout the observational domain and the product generated by the algorithm can be compared directly to model output. An independent test of the algorithm on data for which high-resolution dual-Doppler observations are available shows that the convective–stratiform separation algorithm is consistent with the physical definitions of convective and stratiform precipitation.

The vertical structure algorithm presents the frequency distribution of radar reflectivity as a function of height and thus summarizes in a single plot the vertical structure of all the radar echoes observed during a month (or any other time period). Separate plots reveal the essential differences in structure between the convective and stratiform echoes.

Tests yield similar results (within less than 10%) for monthly rain statistics regardless of the technique used for estimating the precipitation, as long as the radar reflectivity values are adjusted to agree with monthly rain gauge data. It makes little difference whether the adjustment is by monthly mean rates or percentiles. Further tests show that 1-h sampling is sufficient to obtain an accurate estimate of monthly rain statistics.

1. Introduction

The advent of operational radars that scan volumetrically and record the radar data digitally presents the opportunity to build climatological datasets of precipitation amount, structure, and type. From a hydrological standpoint, measurements of precipitation amount with high spatial resolution and coverage are essential (e.g., Smith and Krajewski 1987; Lovejoy and Schertzer 1990; Gupta and Waymire 1990). From a meteorological viewpoint, the vertical and horizontal structures of radar echoes are important indicators of the organization of the cloud systems producing precipitation (e.g., Houze et al. 1976; Houze et al. 1990). From a cloud-physics perspective, it is important to distinguish between convective and stratiform precipitation, which are characterized by different precipitation growth mechanisms (Houghton 1968; chapter 6 of Houze 1993). Distinguishing between convective and stratiform precipitation is also important from a thermodynamic viewpoint, as the vertical distribution of diabatic heating processes are distinctly different in convective and stratiform precipitation regions (Houze 1982, 1989; Johnson 1984).

The Next Generation Weather Radar (NEXRAD) systems currently being installed in the United States (Crum and Alberty 1993; Crum et al. 1993) are archetypical of operational weather radars being installed at locations around the world. By the year 2000, such radars will be in wide use and will form the basis for climatological documentation of precipitation at representative locations over the globe. To be prepared for this opportunity, robust data management and analysis techniques must be developed to extract the climatological information from the operational data.

The rates at which data are collected at modern operational radar sites are high. At a NEXRAD site, three-dimensional volume scans are completed every 5–10 min during precipitation. To derive a manageable climatology of the precipitation type, structure, and amount, we must digest and distill these data. This paper presents and tests a methodology for this purpose. From the data of a volume-scanning operational radar

Corresponding author address: Dr. Matthias Steiner, Atmospheric Sciences, University of Washington, Box 351640, Seattle, WA 98195. E-mail: steiner@atmos.washington.edu

and an associated rain gauge network, we extract the following three types of information:

(i) convective and stratiform regions are separated objectively,
(ii) the vertical structure of the radar echoes is determined statistically, and
(iii) precipitation amount is determined at high (2 km) horizontal resolution.

Algorithms for each of these operations are presented and tested on a 1-month set of data collected in an operational mode at Darwin, Australia. One of the motivations for this study is to provide a methodology that can be used to create climatological products from the radar and rain gauge data collected at validation sites for the Tropical Rainfall Measuring Mission (TRMM) satellite to be launched in 1997 (Simpson et al. 1988; Simpson 1988). Darwin is one of the primary validation sites for TRMM, and our study is, in part, a pilot study for TRMM validation. Although our methodology is quite generally applicable to any state-of-the-art operational radar site, we wish to determine specifically how it will perform for Darwin.

2. Setting for the test—Darwin, Australia, February 1988

Darwin lies just south of the tropical "maritime continent," defined as the islands and seas of the Indonesian–Malaysian archipelago (Ramage 1968). The region has a monsoonal climate (Holland 1986; Keenan et al. 1988). The rainy season normally begins during late December and extends through March. The mean large-scale flow consists of a cyclonic gyre in the lower troposphere and an anticyclonic gyre in the upper troposphere. The general pattern undergoes synoptic-scale spatial and temporal variations accounting for the "break" and "active" periods of the monsoon.

During active periods, the center of the cyclonic gyre is near or south of Darwin, and the low-tropospheric flow on the north side of the cyclone has a long westerly oceanic fetch. The period 8–15 February 1988 was such a monsoonal period. The percentage high cloudiness (PHC)[1] based on the 235-K threshold applied to Geostationary Meteorological Satellite (GMS) infrared (IR) satellite data and the European Centre for Medium-Range Weather Forecasts (ECMWF) 850-hPa mean winds show the persistent high cloudiness and the westerly flow over the ocean just north of Darwin (Fig. 1a). During this time, precipitation in the vicinity of Darwin (determined from the rain gauge network described below) was heaviest (Fig. 2a) and most widespread (i.e., affected the most gauges, Fig. 2b).

During breaks in the monsoon, the cyclonic gyre is centered north of Darwin, and a dry continental flow dominates the region around Darwin. The period 19–26 February 1988 was a break period (Fig. 1b). The cyclonic gyre was extremely weak, and the cloudiness was minimal over the monsoon region as a whole. Nonetheless, the region around Darwin received heavy and widespread rain on four days during this break period (Fig. 2).

The precipitation seen on the Darwin radar is of three main types. 1) During active monsoon periods, the precipitation typically occurs in oceanic mesoscale convective systems (MCSs), which consist of ensembles of convective lines and stratiform regions (Mapes and Houze 1992, 1993). These systems are similar to the tropical oceanic MCSs observed in GATE[2] (Houze and Betts 1981) and MONEX[3] (Johnson and Houze 1987). 2) During break periods, the precipitating cloud systems are less frequent and are typical of a continental origin. They may be intense and are often in the form of squall lines with trailing stratiform precipitation (e.g., Drosdowsky 1984). 3) Over Bathurst and Melville Islands to the north of Darwin (Fig. 3), pronounced diurnally forced thunderstorms locally known as "hectors" occur (Keenan et al. 1989; Keenan et al. 1990; Simpson et al. 1993). Keenan and Carbone (1992) discuss many of the precipitation systems observed in the vicinity of Darwin.

February 1988 was a suitable period for a test based on data from the Darwin area. Substantial precipitation occurred during both active monsoonal and break periods, and hectors occurred over the islands throughout the month.

3. The test dataset

During February 1988, the Darwin site (Fig. 3) was equipped with the National Oceanic and Atmospheric Administration (NOAA) TOGA[4] Doppler radar (5-cm wavelength, 1.65° beamwidth). The radar was located at Berrimah (12°27′26″S, 130°55′31″E), about 20 km east-southeast of Darwin; the radar site is 30 m above mean sea level (MSL).[5] The surrounding rain gauge network, operated by the Australian Bureau of Meteorology (BMRC), consisted of 22 tipping-bucket rain gauges, which were more or less evenly distributed with range from the radar (Fig. 3, Table 1). The rain gauge data were archived in 1-min time resolution at the National Aeronautics and Space Administration

[1] Percentage high cloudiness is defined as the percentage of all the pixels at a given location that have a brightness temperature below a specified threshold temperature over a certain time period.

[2] GARP (Global Atmospheric Research Program) Atlantic Tropical Experiment. Its field phase was in 1974.

[3] Monsoon Experiment. Also part of GARP; its field phases were in 1978–79.

[4] Tropical Ocean Global Atmosphere Program. A 10-year program of atmospheric and oceanic observations that started in 1985.

[5] All heights given in this paper are relative to the mean sea level (MSL).

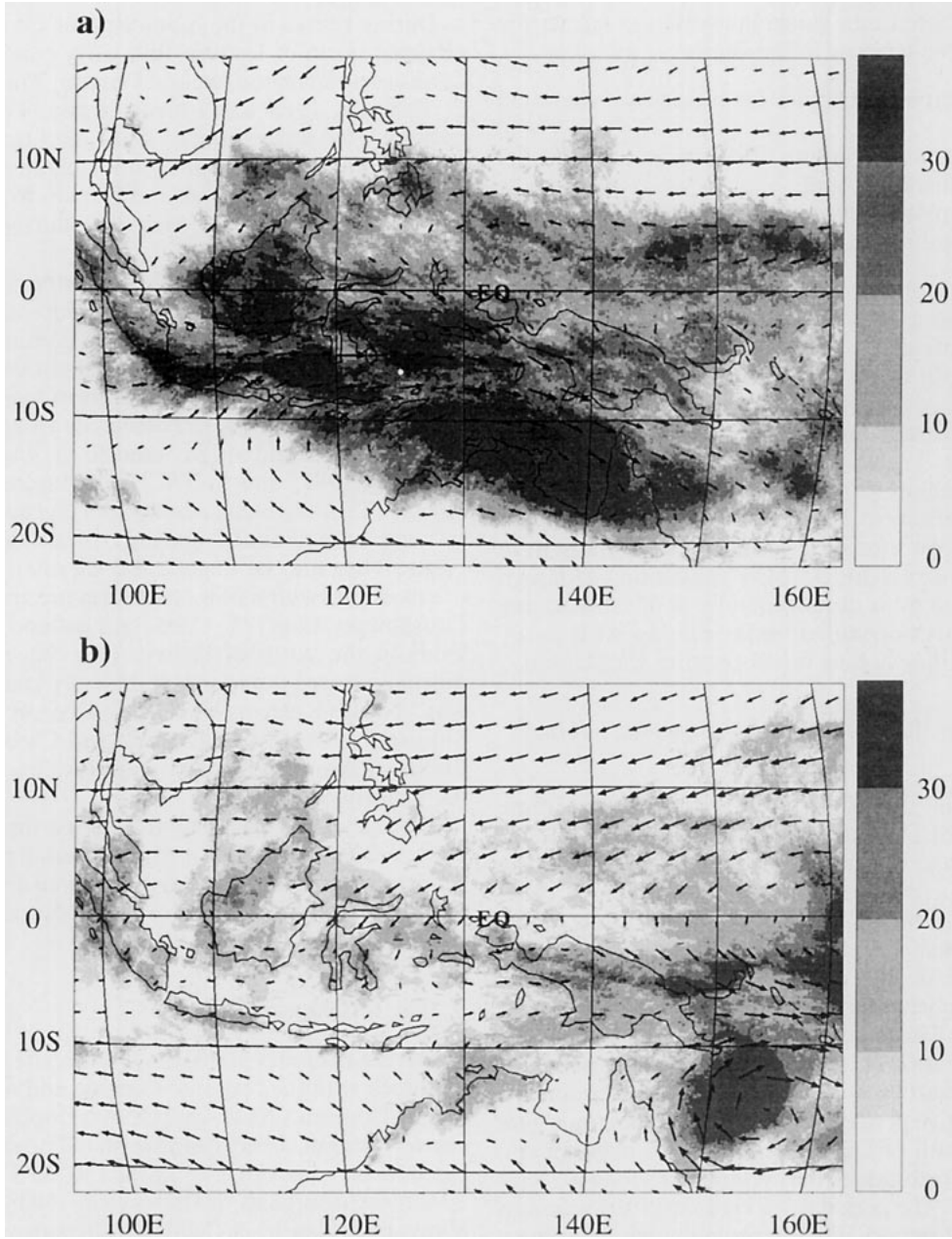

FIG. 1. Percentage of high cloudiness (PHC) less than 235 K based on GMS IR satellite observations (10-km resolution) over the maritime continent. The mean ECMWF 850-hPa wind field pattern (2.5° resolution) is overlaid for the same time period. The wind vector scale is 20 m s^{-1} for an arrow 2.5° in length. Darwin is located at 12°23′S, 130°44′E. (a) Monsoon-type period of 8–15 February 1988, and (b) break-type period of 19–26 February 1988.

(NASA) Goddard Space Flight Center as part of the TRMM ground-truth program (Thiele 1988; Thiele et al. 1992). Rawinsonde soundings were taken every 6 h at Darwin during February 1988. Further description of the radar installation and the rain gauge network can be found in Keenan et al. (1988), Rosenfeld et al. (1993), and Short et al. (1993).

The radar calibration was checked electronically every few days. Several times a year the radar was calibrated with a metal sphere of known cross section flown on a balloon 3 km away from the radar site. Typically, the radar reflectivities agreed within 1–2 dB with those expected from the metal sphere (T. Keenan 1992, personal communication; see also appendix of Simpson et al. 1993).

Table 2 summarizes the scan strategies of the Darwin radar for February 1988. Three-dimensional data are obtained by scanning the radar through a series of full

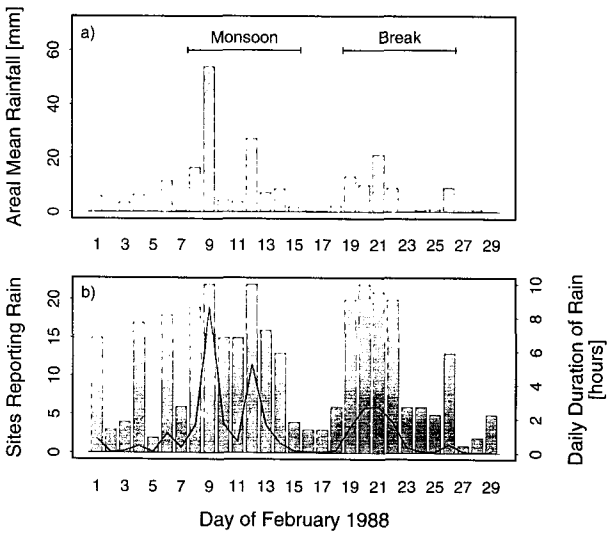

FIG. 2. Rain gauge–based daily mean rainfall information for February 1988 at Darwin. (a) Areal mean rainfall accumulation. The monsoon and break periods corresponding to Fig. 1 are indicated. (b) Number of rain gauge sites (maximum 22 sites) that reported rain on a given day (histogram), and daily duration of rainfall (maximum 24 h) recorded by the rain gauge network at Darwin (curve).

azimuth revolutions at increasing elevation angles. We use the 12-elevation (tilt sequence) volume scans recorded at approximately 0330, 0930, 1530, and 2130 LST (local standard time = UTC + 9.5 h). A total of 116 volume scans were obtained at these times, but 10 had to be withdrawn because of the quality of the recorded raw data (i.e., hardware problems), so the analysis is based on 106 volumes of radar data.

4. Data processing and analysis flowchart

Figure 4 shows a flowchart of the steps we follow in processing an individual radar volume scan. The raw reflectivity data obtained by scanning the radar through a tilt sequence are in spherical coordinates (azimuth, elevation, and range). They are subjected to quality-control editing to remove echoes produced by ground clutter, anomalous propagation, and range aliasing (e.g., Rinehart 1991). The edited data are then interpolated to a three-dimensional Cartesian grid. We describe the editing and interpolation procedures in section 5.

The Cartesian-gridded reflectivities are used as input to algorithms that result in products describing the instantaneous reflectivity field and its associated precipitation. In this paper, we describe algorithms for (i) separating the convective and stratiform components of the radar echo pattern (section 6), (ii) characterizing the vertical structure of the echoes (section 8), and (iii) relating the reflectivity field to rain rates (section 10). *These algorithms are independent; they may be applied either separately or in combination.* In sections 7–9 we apply and verify the convective–stratiform separation algorithm. In section 11, we describe the variability of the monthly rainfall in terms of area covered by precipitation and total rainfall amounts within land–ocean and convective–stratiform categories.

5. Editing and interpolation of the radar data

The quality-control editing for this study was done interactively with the aid of the Research Data Support System software (RDSS; Brown and Borgogno 1980; Oye and Carbone 1981) developed and maintained by the National Center for Atmospheric Research (NCAR). Future work will employ fully automated editing. As a test of the sensitivity of the results to the editing, the entire data analysis presented in this paper was done twice, once using the edited and then using the unedited radar volume scans. The unedited reflectivity data produced a 16% larger monthly radar echo coverage and an 11% increase in areal rainfall compared to the edited data. The spatial distribution of the error is illustrated in Fig. 5. Second-trip (range-folded) echoes occurred randomly, equally over ocean and land. The low-elevation scans usually exhibited ground clutter echo out to ranges of approximately 50 km. However, at these ranges the Cartesian gridded data at the 3-km altitude—the level of analysis for the con-

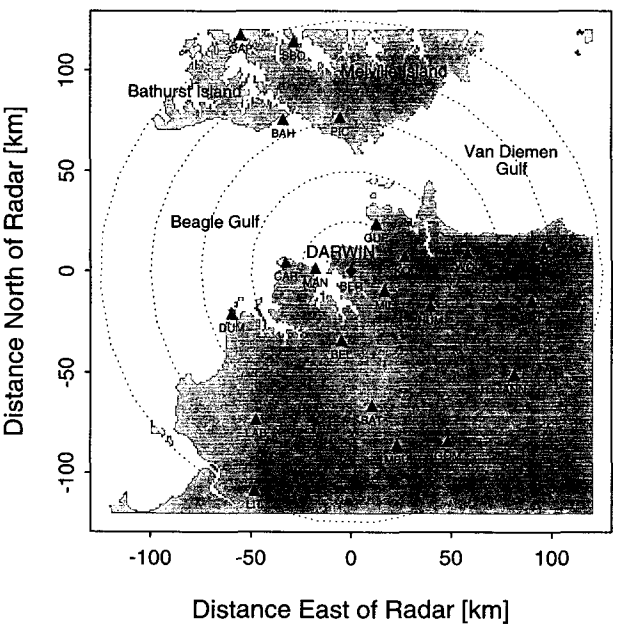

FIG. 3. Geographical map of the Darwin region including the radar and rain gauge sites. The domain shown (240 km × 240 km) represents the area of interest to the present study. The NOAA TOGA Doppler radar, indicated by the solid diamond in the center of the figure, is located at Berrimah (BER). The dotted range rings indicate distance from the radar site at 25-km intervals. The positions of the rain gauge sites are shown by solid triangles and labeled by their acronyms (Table 1).

TABLE 1. Rain gauge network in the vicinity of the Darwin radar site, valid for February 1988. Berrimah is the location of the NOAA TOGA radar installation. The rain gauge locations are expressed relative to the radar site in both a polar and Cartesian coordinate system having the radar site as its center point. For the exact geographical locations (lat/long) of the rain gauge sites see Short et al. (1993). The continuous gauge-based rainfall accumulations for February 1988 are listed for each site as well as the radar-estimated monthly rainfall at that site using the gauge-adjusted GATE Z–R relation (for further details see section 10a).

Rain gauge site	Short	Direction	Distance (km)	x (km)	y (km)	Gauge (mm)	Radar (mm)
Annaburroo	ANN	122°	96	81.4	−50.9	263.1	163.4
Batchelor Airstrip	BAT	171°	67	10.5	−66.2	179.5	135.5
Bathurst Island	BAH	336°	83	−33.8	75.8	195.0	203.0
Bellville Park	BEL	188°	34	−4.7	−33.7	227.8	224.1
Berrimah	BER	0°	0	0	0	326.2	—
Charles Point	CAR	278°	33	−32.7	4.6	176.6	84.3
Dum In Mirie	DUM	251°	63	−59.6	−20.5	220.3	247.8
Garden Point Airstrip	GAP	335°	130	−54.9	117.8	310.8	685.9
Goodall Mine	GOM	150°	97	48.5	−84.0	295.7	45.5
Gunn Point Prison	GUP	28°	27	12.7	23.8	233.4	221.3
Humpty Doo Navy	HUM	113°	43	39.6	−16.8	268.4	153.9
Koolpinyah	KOL	75°	28	27.0	7.2	239.4	199.5
La Belle Airstrip	LAB	213°	87	−47.4	−73.0	228.8	126.0
Litchfield	LIT	204°	119	−48.4	−108.7	149.6	94.8
Mandorah Jetty	MAN	275°	18	−17.9	1.6	195.2	91.7
McMinns Lagoon	MIL	119°	19	16.6	−9.2	204.5	277.0
Mt. Bundy	MBU	165°	89	23.0	−86.0	267.0	519.8
Old Point Stuart	OPS	83°	97	96.3	11.8	174.3	157.4
Pickertaramoor	PIC	356°	77	−5.4	76.8	260.1	179.2
Point Stuart Abattoirs	PST	99°	91	89.9	−14.2	154.4	83.2
Snake Bay Old	SBO	346°	118	−28.5	114.5	68.3	567.7
Woolner	WOL	81°	59	58.3	9.2	309.1	151.3
Areal mean rainfall	(including Berrimah = radar site)					224.9	—
	(without Berrimah)					220.1	219.6

vective–stratiform separation (section 6c) and surface rainfall estimation (section 10)—are not based on the lowest elevation angles. At distances greater than about 90 km from the radar site—especially over the southern and southeastern part of the study area—anomalous propagation, caused by temperature inversions, falsely produced more rainfall in the unedited radar data. At these ranges, the 3-km altitude Cartesian-gridded data are derived almost entirely from the low elevation angles. The most crucial editing was, therefore, that required to remove the anomalous propagation echoes.

After the radar data have been edited, they are bilinearly interpolated into a Cartesian grid by means of the NCAR Sorted Position Radar Interpolation software (SPRINT; Mohr and Vaughan 1979). The azimuthal and vertical resolution of the 1.65° Darwin radar beam exceeds 1.5 km at ranges larger than 50 km and reaches 3 km at a distance of approximately 100 km. We interpolate to a Cartesian grid, which is as close as possible to the average spatial resolution of the radar data. For most of this study, we use a 240 km × 240 km Cartesian grid centered on the radar with a 2-km horizontal and 1.5-km vertical resolution. For some comparisons, we also use a grid with 4-km horizontal and 3-km vertical resolution.

TABLE 2. Radar scan strategies for the February 1988 observation period at Darwin. The basic scan strategies comprise 360° sweeps at constant elevation angles (plan position indicator, PPI) and vertical cross-section sweeps in a given direction (range–height indicator, RHI). Several successive PPIs at increasing elevation angles are generally combined into volume scans. Note, the base scan PPI is done using a different pulse repetition frequency (PRF) and pulse length than the volume scans.

Scan type	PRF (s^{-1})	Pulse (s)	Elevations	Elevation angles
PPI (base scan)	400	2×10^{-6}	1	0.8°
PPI (partial volume scan)	841	0.5×10^{-6}	3	0.8°, 2.5°, 4.0°
PPI (volume scan, low)	841	0.5×10^{-6}	12	0.8°, 2.5°, 4.0°, 5.4°, 6.8°, 8.3°, 10.0°, 12.1°, 14.3°, 17.3°, 20.8°, 25.0°
PPI (volume scan, high)	841	0.5×10^{-6}	7	30.0°, 35.0°, 40.0°, 45.0°, 50.0°, 55.0°, 60.0°
PPI (vertical scan)	841	0.5×10^{-6}	1	90.0°
RHI	841	0.5×10^{-6}		0°–60° elevation, variable azimuth directions

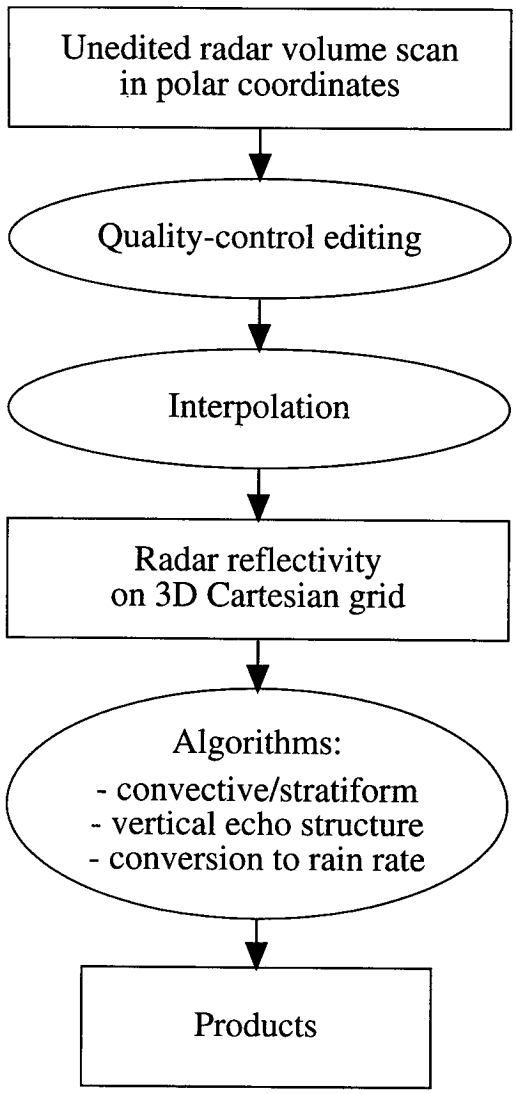

FIG. 4. Analysis flowchart showing the processing steps for each radar volume scan.

6. Identification of convective and stratiform precipitation echoes

a. *Physical differences between convective and stratiform precipitation*

The first algorithm we apply to the three-dimensional Cartesian-gridded radar echo field (Fig. 4) separates the echo into its convective and stratiform components. Definitions of stratiform and convective precipitation are given by Houze (1993, chapter 6).[6] Houghton (1968) pointed out that the microphysical distinction between stratiform and convective precipitation lies in the magnitude of the in-cloud vertical air motions and the timescale of the microphysical precipitation growth processes. Most stratiform precipitation falls from clouds that reach well above the 0°C level,[7] and ice particles in the upper levels of the cloud play an important role in the precipitation process.

Stratiform precipitation is defined to exist when the vertical air motion satisfies the condition

$$|w| \ll |V_t|, \tag{1}$$

where V_t is the terminal fall velocity of snow particles ($\sim$1–3 m s^{-1}). Under this condition, ice particles in the upper levels of the clouds must fall; they cannot be suspended or carried aloft by the air motions as they grow. It follows that all the growth of the precipitating particles must occur while they are falling. At higher levels, the ice particles grow mainly by vapor deposition. When they descend to within about 2.5 km of the 0°C level, aggregation and riming can occur. The aggregation is most frequent within about 1 km of the 0°C level (e.g., Hobbs 1973; Houze and Churchill 1987). Aggregation concentrates the condensate into large particles, which, upon melting, become large, rapidly falling raindrops. The layer in which the large snowflakes melt is often evident on radar by a bright band of intense echo in a horizontal layer about 0.5 km thick located just below the 0°C level (Ryde 1946; Austin and Bemis 1950; Wexler and Atlas 1956; Battan 1959, 1973). The bright band, however, is not always evident on radar since the vertical resolution is usually incapable of resolving it except close to the radar, and at the early stages of development of the stratiform precipitation the bright band may not yet be evident even though (1) may be satisfied through most of the radar echo volume (Yuter and Houze 1995a,b,c).

Convective precipitation processes differ sharply from stratiform processes. The vertical air motion violates condition (1); $w \sim$ 1–10 m s^{-1} or more, which equals or exceeds the typical fall speeds of ice crystals or snow. Precipitation particles grow primarily by accretion of liquid water. Aircraft observations of ice particles in the upper levels of convective clouds commonly show that the particles in the updrafts grow by riming (e.g., Matejka et al. 1980; Heymsfield and Musil 1982; Knight et al. 1982; Dye et al. 1983; Churchill and Houze 1984; Houze and Churchill 1984; Waldvogel et al. 1987). Since the strong updrafts in convective clouds are usually narrow and can loft large particles upward, radar echoes associated with active convection form well-defined vertical cores of maximum reflectivity, which contrast markedly with the horizontal orientation of the radar bright band seen at the melting level in stratiform precipitation.

[6] A definition of stratiform precipitation is not given in the *Glossary of Meteorology* (Huschke 1959).

[7] Drizzle or light rain from warm stratus or stratocumulus might also be considered a type of stratiform rain. However, such warm stratiform rain is not a significant contributor to global rainfall and is not considered here.

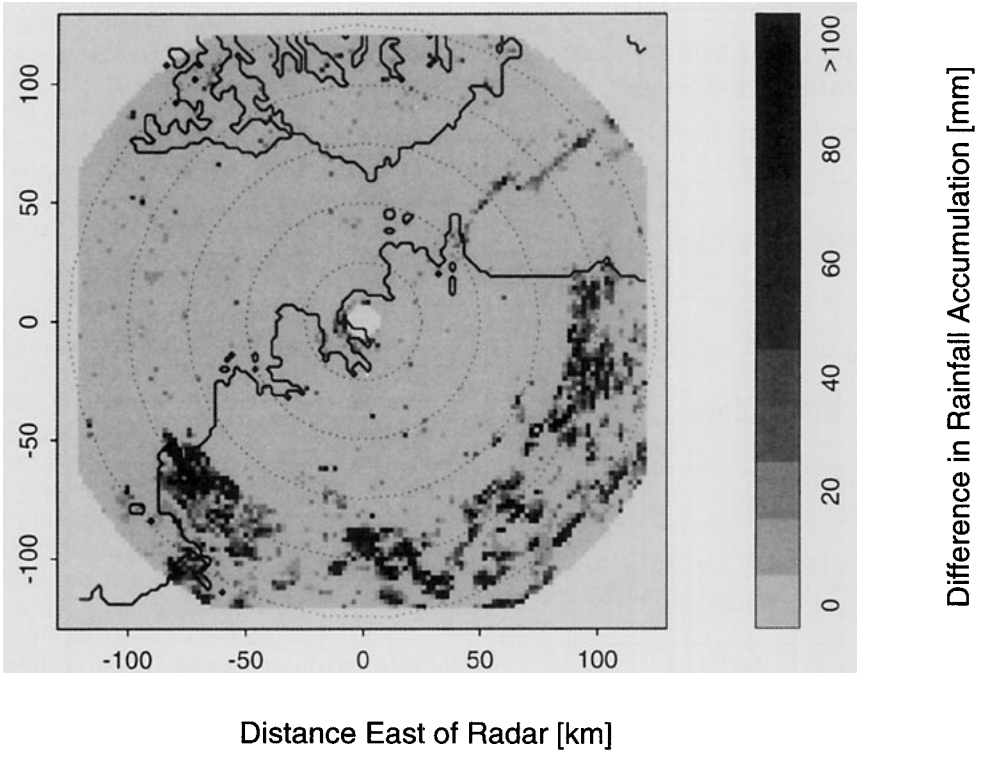

FIG. 5. Difference in the monthly rainfall accumulation of unedited versus edited radar data for February 1988 in the vicinity of Darwin, Australia. Except for the quality-control editing step, the edited and unedited radar volumes are processed identically using the same Z–R relation. The geographical contours are outlined (heavy line). The range rings (dotted circles) indicate distance from the radar site at 25-km intervals.

b. Methods for distinguishing between stratiform and convective precipitation in radar echo patterns

1) VERTICAL VELOCITIES AND BRIGHTBAND METHODS—NOT OPERATIONALLY USEFUL

Several approaches have been tried to distinguish convective and stratiform precipitation in radar data. Since the physical distinction lies in the vertical velocity condition (1), data on vertical motions would be ideal. However, vertical velocity information is not available operationally. Therefore, we use radar reflectivity structure as a proxy to indicate whether or not condition (1) is satisfied.

Some methods use the radar reflectivity bright band to identify stratiform precipitation (Collier et al. 1980; Rosenfeld et al. 1995). However, this approach is severely limited for two reasons:

1) Because the radar beam widens with distance from the radar, the vertical resolution of the data are adequate to distinguish the bright band only at near range[8]—usually less than 100 km (Andrieu and Creutin 1995), depending on the radar beamwidth. This limitation severely reduces the area over which the bright band can be detected, and any algorithm using this criterion is thus dependent on the location of the radar with respect to the precipitation. This limitation is reduced in the case of airborne (e.g., NOAA WP-3D tail Doppler radar and the ELDORA system mounted on the NCAR Electra) or spaceborne radars (TRMM precipitation radar) since these platforms move across areas of precipitation while scanning either in a vertical cross-section mode or by looking downward through the precipitation. A brightband identification may be more useful for such radars on moving platforms. However, for any ground- or ship-based radar this approach is not robust.

2) The bright band is only well defined when the stratiform precipitation is well developed. Regions in which stratiform precipitation is in an early or late stage of development or where stratiform precipitation is in-

[8] Since the bright band typically has a vertical extent of only a few hundred meters (Matsuo and Sasyo 1981; Steiner and Waldvogel 1989; Fabry et al. 1994), the vertical resolution of the radar beam should be comparable to clearly distinguish the bright band. A radar with a 1.5° beamwidth has a vertical resolution of 1.5 km at a distance of 60 km and at least 3 km at ranges of 120 km and farther. Though a maximum in the vertical reflectivity profile might be recognized at the melting level out to ranges of maybe 100 km, it is not necessarily a brightband signature that has been observed. For example, embedded convection could easily be mistaken for a bright band at coarse vertical resolution.

termingled with convective precipitation often do not clearly exhibit a bright band (e.g., chapter 11 of Rogers 1979; Houze and Betts 1981; Yuter and Houze 1995b).

For these two reasons, a method that identifies only the brightband regions as stratiform and classifies the remainder of the precipitation as convective will underestimate the stratiform component of the precipitation and overestimate the convective part. *Observation of a bright band is a sufficient but not a necessary condition for a region to be stratiform.* Overemphasis of the bright band as a criterion could partially explain the low percentage of stratiform precipitation found by Rosenfeld et al. (1995).

The observation of a bright band may be used as a *check* to assure that a region with a bright band is not falsely identified as convective (see section 6d), but it cannot be used as the sole criterion to determine whether a region is stratiform.

2) HORIZONTAL RADAR ECHO STRUCTURE

Since vertical velocities are generally not available and brightband methods are limited in applicability, the horizontal structure of precipitation is the only remaining criterion on which to base a convective–stratiform separation algorithm. Several techniques have been tried.

Time continuity can be useful. If a system maintains an archetypical squall-line structure over a period of time, the leading convective and trailing stratiform regions can be identified and tracked semi-objectively (Houze 1977; Gamache and Houze 1982, 1983; Houze and Rappaport 1984; Wei and Houze 1987; Chong and Hauser 1989; Rutledge and MacGorman 1988; Biggerstaff and Houze 1991; Johnson and Hamilton 1988). However, this approach is limited to a particular type of storm. Cheng and Houze (1979) and Leary (1984) used time continuity to determine if an echo pattern was fluctuating rapidly or slowly in time. If a pattern showed both small-scale spatial and temporal variability it was dubbed convective. Other precipitation was defined as stratiform. This technique is laborious and computationally intensive since all echoes must be tracked in time. It is therefore impractical for a large operational dataset.

A simpler and more practical method of distinguishing between convective and stratiform precipitation is to use the *horizontal structure of the precipitation field.* Houze (1973), Churchill and Houze (1984), and Steiner and Houze (1993) have developed such a method. The algorithm we describe and test in this paper is the latest refinement of this technique. The basic idea of this method, which is fully automated, is to search for peaks of rain rate (or reflectivity). If the peaks satisfy specified criteria regarding the ratio of the peak rain rate to the surrounding background rain rate, then the peaks (plus a specified surrounding rain area) are categorized as convective. After all peaks and surrounding areas have been located and identified as convective, the remainder of the precipitation is categorized as stratiform. Since this method searches for convective precipitation and defines the remainder as stratiform, it differs fundamentally from a method employed by Rosenfeld et al. (1995), which uses the brightband signature to classify precipitation. The Rosenfeld method implicitly searches for stratiform precipitation and defines the remainder as convective.

Steiner and Houze (1993) slightly modified the Churchill and Houze (1984) separation technique to work with the reflectivity field, searching for pixels that have radar reflectivity exceeding the background by 4.5 dB (which corresponds approximately to the factor of 2 in rain rate used by Churchill and Houze). This procedure allows the separation of stratiform and convective rain areas to be done before any Z–R relationship is applied to convert the echo field to a rain rate field. *This order of analysis and computation makes the convective–stratiform separation algorithm completely independent of whatever technique is used to convert the reflectivity to rain rate.*

c. *The improved method for separating stratiform and convective radar echoes*

The study of Steiner and Houze (1993) showed that 1) a convective–stratiform separation methodology of the type designed by Churchill and Houze (1984) is sensitive to the horizontal spatial resolution of the data. 2) The Churchill and Houze scheme tends to overestimate the area identified as convective precipitation. The latter finding was obtained by applying the Churchill and Houze scheme to the Darwin February 1988 data and then visually inspecting the three-dimensional structure of many single radar volumes. Several echo cores in the range of 20–30 dBZ were classified as convective even though they exhibited a well-defined brightband signature. To overcome this tendency and to apply the technique on a 2-km grid resolution, we have further modified the separation technique.

The revised criteria for identifying convective precipitation are

- *Intensity:* Any grid point in the radar reflectivity field with reflectivity of at least 40 dBZ is automatically labeled as a convective center, since rain of this intensity could practically never be stratiform.
- *Peakedness:* Any grid point in the radar reflectivity field not identified as a convective center in the first step, but which exceeds the average intensity taken over the surrounding background by at least the reflectivity difference depicted in Fig. 7 is also identified as a convective center. The background intensity is determined as the linear average of the nonzero radar echoes ($mm^6\ m^{-3}$) within a radius of 11 km around the grid point (Fig. 6a). The area covered by the circle is roughly the same as the square regions used by Churchill and Houze (1984): roughly 400 km^2.

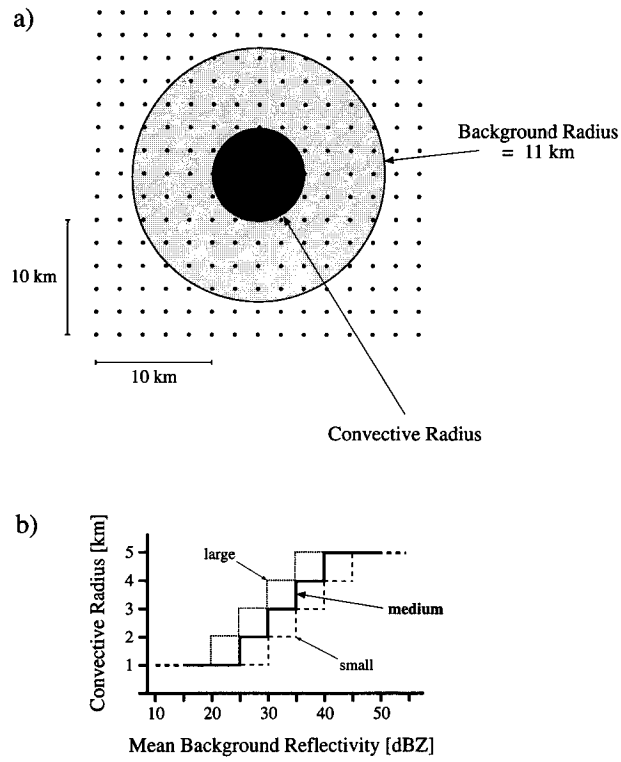

FIG. 6. (a) Schematic diagram showing how convective grid points are identified. The lightly shaded circular area indicates the area within the background radius surrounding a given grid point (bold point in the center of the figure). The darker-shaded area represents the area around the convective center—if identified as such—that is included as convective area. The radius of this convective area is a function of the average reflectivity within the background radius. (b) The convective area radius as a function of the mean background reflectivity. Three different relations are tested (large—dotted, medium—heavy, small—dashed line) as discussed in the text. Dots are spaced 2 km apart corresponding to Cartesian grid resolution of the radar data.

• *Surrounding area:* For each grid point identified as a convective center by one of the above two criteria, all surrounding grid points within an intensity-dependent convective radius around that grid point are also included as convective area (Fig. 6b).

The separation is performed on Cartesian-gridded reflectivity data at 3-km altitude, which is high enough to provide radar data out to ranges of about 140 km and still low enough not to be seriously affected by the brightband signature—the 0°C level in the Tropics is usually around 5-km altitude. In the environment of Darwin, evaporation between the surface and 3 km does not significantly change the precipitation pattern at those levels.[9] In midlatitudes, characterized by a much more variable height of the 0°C level and sometimes significant evaporation, the convective–stratiform separation technique will have to be applied at a lower level.

The reflectivity difference by which a given radar echo must exceed the background intensity in its local environment to become identified as a convective center (Fig. 7) has been tuned for the radar data collected during February 1988 at Darwin, Australia. Vertical and horizontal cross sections in 18 of the 106 radar volume scans were inspected to determine the stratiform and convective parts of the precipitation systems. The radar volumes selected represent all the major rainfall events that occurred during February 1988. The objective convective–stratiform separation method has been iteratively adjusted to match the manual identification as closely as possible. The result is the curve shown by the solid line in Fig. 7. This curve is the difference ΔZ between the reflectivity at a grid point and the background reflectivity Z_{bg}, which must be exceeded for the grid point to be designated as a convective center in the second step above. The curve is given by

$$\Delta Z = \begin{cases} 10, & Z_{bg} < 0 \\ 10 - Z_{bg}^2/180, & 0 \leqslant Z_{bg} < 42.43, \\ 0, & Z_{bg} \geqslant 42.43 \end{cases} \quad (2)$$

where ΔZ is in decibels and Z_{bg} in dBZ. For comparison, the convective center peakedness criteria used by Churchill and Houze (1984) and Steiner and Houze (1993) are also shown in Fig. 7.

Figure 8a shows an example of a horizontal radar reflectivity pattern collected at Darwin with the areas

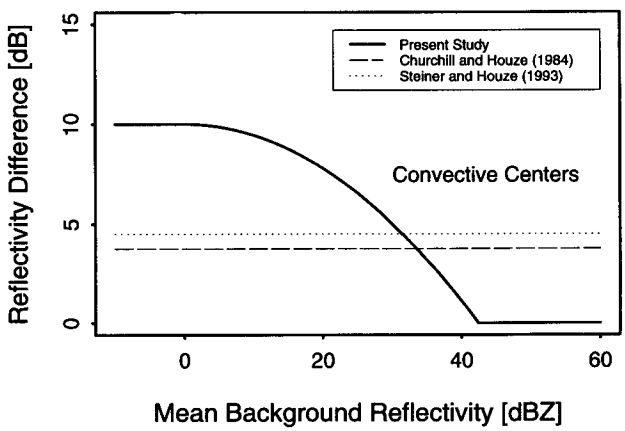

FIG. 7. Peakedness criteria—i.e., reflectivity difference between the gridpoint and mean background—used for convective center identification. In the present study (solid curve), the peakedness criterion is a function of the mean background reflectivity. Points along and above this curve are classified as convective centers. The constant peakedness criteria used by Churchill and Houze (1984) and Steiner and Houze (1993) are indicated by the dashed and dotted lines, respectively.

[9] The effect of evaporation is strongest on the smallest droplets, while the radar reflectivity and rain rate are determined mainly by the larger drops.

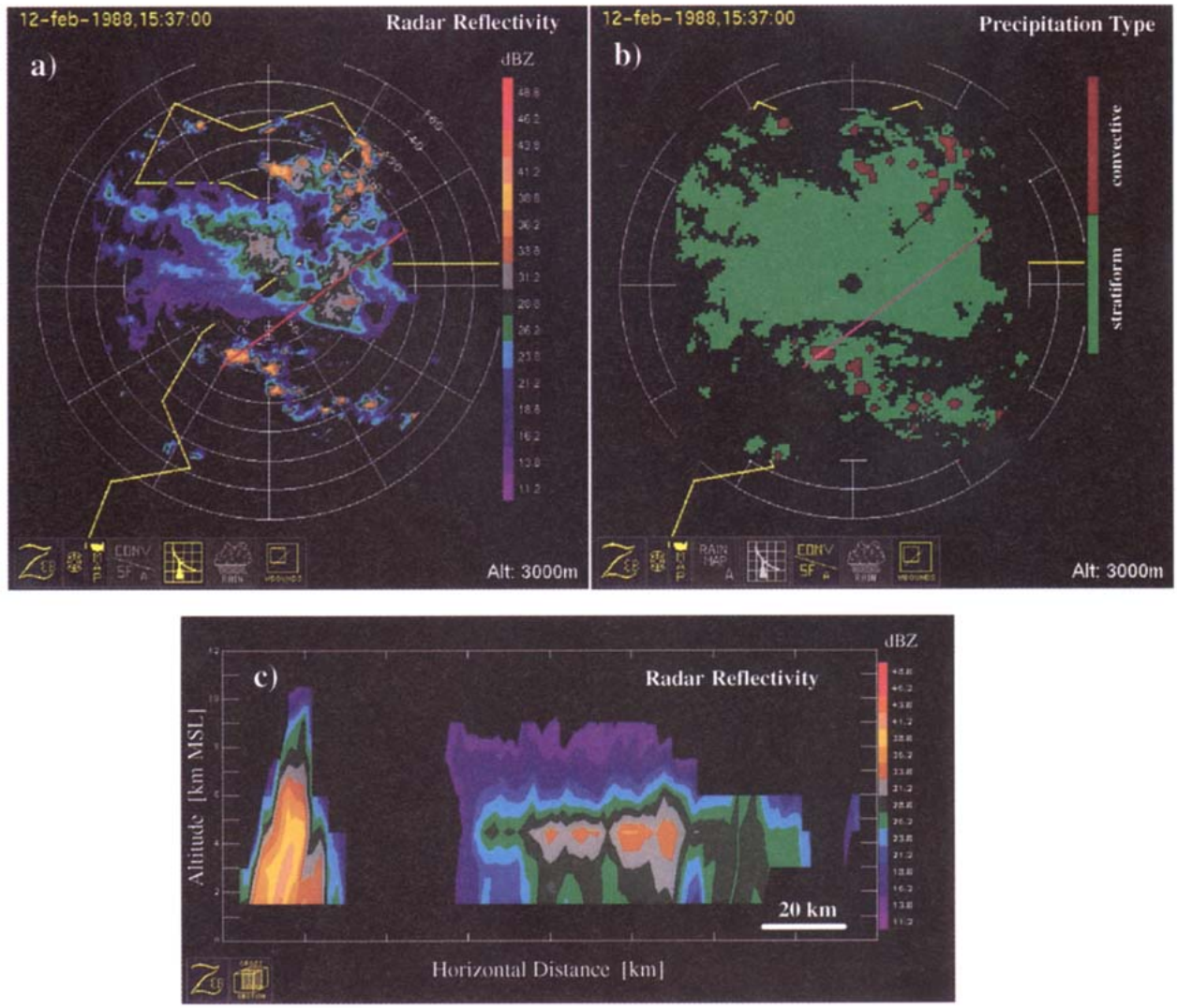

FIG. 8. (a) Horizontal radar reflectivity field at the 3-km altitude, and (b) areas identified as convective (red) and stratiform (green) by the objective separation algorithm. The radar volume scan shown was recorded at Darwin, Australia, on 0607 UTC (1537 LST) 12 February 1988. The red line indicates the position of the vertical cross section shown in Fig. 8c. The cross section has a horizontal extent of 160 km.

identified by the separation algorithm as convective and stratiform, indicated in Fig. 8b. The vertical cross section along the solid line in Figs. 8a and 8b is shown in Fig. 8c. The region identified as convective at about 50–60 km south-southwest of the radar appears as a distinctly vertically oriented reflectivity maximum in the vertical cross section, while the region classified as stratiform (to the east of the radar) exhibits a radar bright band across most of its breadth.

The iterative tuning to obtain the curve in Fig. 7 for Darwin, February 1988, *calibrates the convective–stratiform separation technique against the vertical structure of radar echoes in regions where it is possible to detect a bright band.* Our algorithm thus minimizes false convective identification while using a technique that is uniformly applied over the whole field of data.

Experience with tuning the convective precipitation identification algorithm for other datasets indicates that both the first (intensity) and second (peakedness) criteria may need to be modified to best distinguish convection for a particular geographic location (precipitation regimes) and radar (scanning strategies, beamwidth, sensitivity, etc.). The third (surrounding area) criterion appears to be primarily a function of grid resolution rather than precipitation regime. Once the convective identification algorithm is tuned for a particular location and radar with a representative dataset, it does not need to be retuned month to month.

d. Sensitivity tests

In this section we examine the sensitivity of the convective–stratiform separation to the grid resolution of

the radar data, and to the size and shape of the convective area surrounding a pixel identified as a convective center. Table 3 lists the versions of the algorithm used to make these sensitivity tests, which are performed on the month-long dataset from Darwin, February 1988.

Cases 1a and 1b represent the Churchill and Houze (1984) version of the convective–stratiform separation method. Case 1a uses the method in its original form (4-km horizontal resolution), while case 1b applies the technique on a 2-km horizontal resolution grid. The background and convective areas are squares centered on the convective core. Cases 2a–e apply the current version of the separation technique under five sets of conditions. For these cases, the background and convective areas are circular. The background area is the set of pixels having their center points within a radius of 11 km of the grid point of investigation (336 km^2 for the 4-km grid and 388 km^2 for the 2-km grid). The radius of the convective area surrounding a convective center is variable, depending on the background reflectivity at the convective center (Fig. 6b). Cases 2a–e differ in the grid resolution and size of convective area. Four convective area sizes are considered. Case 2b includes only the convective center pixel in the convective area. In cases 2c–e, we denote the convective area size as small, medium, or large according to Fig. 6b.

Examination of vertical cross sections such as in Fig. 8c suggests that case 2d is the most reliable separator of convective and stratiform echoes for a 2-km resolution grid (further discussion below and in section 9). Most of the results presented in this paper are therefore based on case 2d. The other cases illustrate the performance of the technique under alternative sets of assumptions.

The convective contributions to the monthly total radar echo area coverage and accumulated areal rainfall that resulted from the various cases investigated are given in Table 3. The convective fractions of the monthly areal rain amount indicated in the table were determined by converting radar reflectivity to rainfall rate by means of the single power-law method [section 10a, Eq. (5)]. Use of a different Z–R relation does not substantially change any conclusions implied by Table 3. The general sensitivity of the results to the choice of Z–R relation is discussed in section 11.

The following results are gleaned from Table 3:

- Cases 1a and 2d compare the Churchill and Houze (1984) method and the basic version of the method introduced in this paper. The difference in the monthly convective rainfall contribution is 7%. However, the convective area contribution is down from 30% to 12% in the present method—that is, the Churchill and Houze method incorporates more light rain area in the convective areas.
- Cases 1a and 2d are the cases in which the algorithm was run on data with the grid resolution the algorithm was designed for. Comparison of cases 1a with 1b and cases 2a and 2d demonstrate the effect of applying these methods to another grid resolution without retuning the algorithm. *When the algorithm is designed for a lower-resolution grid, it identifies too much area as convective if run on a higher grid resolution, since the higher-resolution data reveal more details in the reflectivity pattern—and vice versa.*
- Cases 2b–e demonstrate the sensitivity of the algorithm to how large a region around a convective center was included as convective area. The inclusion of no area around the convective cores (case 2b)—using only the identified convective center pixel—resulted in just 3% of the monthly total area coverage and less than 40% of the one-month rainfall accumulation identified as convective. Including a small region surrounding the convective center raised the convective rain fraction to 54%. An extremely large area around the convective cores (case 2e) produced a convective rainfall fraction of 62%. Our best estimate (case 2d) of the convective rainfall contribution is approximately 60% for the Darwin February 1988 data.

The sensitivity of the calculated monthly convective rain amount to the prescribed size of the convective rain area surrounding each convective center seen by comparing cases 2b–e indicates that this parameter must be accurately calibrated for the overall methodology to be accurate. We use the vertical structure of the radar echo as a check on the accuracy of the tech-

TABLE 3. Summary of the convective–stratiform separation algorithms tested in this study. The cases differ in grid resolution, shape of background area, and size of the convective area included around a pixel identified as a convective core by the separation algorithm. The conversion of the radar reflectivity to rainfall rate is with the single power law in Eq. (5).

Case	Grid resolution hor./vert. (km)	Background area	Convective area	Convective fraction of echo area	Convective fraction of rain volume
1a	4/3	20 km × 20 km	12 km × 12 km	30%	66%
1b	2/1.5	22 km × 22 km	10 km × 10 km	43%	77%
2a	4/3	11-km radius	medium	7%	47%
2b	2/1.5	11-km radius	1 pixel only	3%	38%
2c	2/1.5	11-km radius	small	9%	54%
2d	2/1.5	11-km radius	medium	12%	59%
2e	2/1.5	11-km radius	large	16%	62%

nique. As noted in section 6b, the presence of a bright band in a vertical profile of radar reflectivity is a sufficient (though not a necessary) condition for an indication that the precipitation is stratiform. Hence, if a region identified by the algorithm as convective contains a brightband signature, the algorithm is in error. We have systematically searched the convective areas identified by our separation algorithm for instances of such false convective identification.

We do not examine cases with a lower-resolution grid (vertical resolution of 3 km) since a vertical resolution of at least 1.5 km is needed to reveal the brightband signature in the Cartesian-gridded radar volumes (Steiner and Houze 1993). For all the cases with 1.5-km vertical resolution (corresponding to a 2-km horizontal resolution), the bright band and its strength have been determined for grid points in the horizontal reflectivity field. Calculations were made only within a 100-km range of the Darwin radar. At greater range, the radar beam cannot resolve a bright band reliably. For each vertical column in the three-dimensional reflectivity volume, it was first determined if the maximum reflectivity occurred within the height range of 3–5.5 km (i.e., at either the 3- or 4.5-km level). If this was the case, the maximum reflectivity was located in the vicinity of 5-km altitude (the 0°C level for February 1988[10]) and likely corresponded to a bright band. The brightband strength was determined by taking the minimum of the difference between the maximum reflectivity and the reflectivity at grid points immediately above and below.

Table 4 shows the percentage of incorrect classification of the precipitation type (i.e., stratiform rainfall falsely identified as convective) with respect to the presence of a brightband signature. The percentages shown in Table 4 represent the number of radar echo pixels classified as convective but exhibiting a clear brightband signature in the reflectivity profile above that pixel, compared to the total number of pixels that showed a bright band in their local vertical reflectivity profile. With the current technique for separating the two distinct precipitation types, but without including any convective area around the cores (case 2b), only 2% of actual stratiform rain area (exhibiting a brightband signature) is falsely identified as convective for the entire month of February 1988. Increasing the size of the area surrounding the convective cores that was included as convective area by the algorithm (cases 2c–e) increased the number of improper classifications. From visual inspections of the radar data, we are most confident of the separation scheme that includes a medium-sized convective area around the cores (case 2d). But, even with a relatively large area included around the grid points identified as convective cores (case 2e), *the current algorithm produces misclassifications less than 10%.*

TABLE 4. Number of pixels with falsely classified precipitation type—i.e., precipitation echoes exhibiting a clear brightband signature that were identified as convective rainfall by the separation algorithm—expressed as a percentage of the total number of pixels that show a bright band in their vertical reflectivity profile. "Working height" is the altitude at which the convective–stratiform separation method is applied.

		Brightband strength	
Case	Working height	>2 dB	>5 dB
2b	3 km	2.2%	1.8%
2c	3 km	5.4%	5.1%
2d	3 km	7.0%	6.4%
2e	3 km	8.6%	8.0%
2d	1.5 km	6.4%	5.8%

This last conclusion is especially significant for TRMM. Tao et al. (1993) suggest that the uncertainty in identifying stratiform and convective precipitation should be less than 10% in order to use the TRMM precipitation data in model-based estimates of the vertical profile of heating associated with tropical precipitation.

Note that we have now used the brightband information, where it is available, to calibrate both the *location* of convective centers and the *size* of the convective area surrounding the center. As a final test, we run the convective–stratiform separation analysis (with a similar configuration as case 2d) on the data at the 1.5-km height level. The results were very comparable to the ones obtained by case 2d; only the result of the brightband check is shown in Table 4. This result suggests that any level below the bright band can be used to make the convective–stratiform separation as long as the data have undergone a quality-control process to remove spurious echoes. The analysis level[11] should be selected in consideration of the radar scan strategy (how much area is covered by radar at a given altitude) and the meteorological conditions of the precipitation regime (0°C level) (sections 5 and 6c).

7. Application of the convective–stratiform separation algorithm to the data of Darwin, February 1988

After the three-dimensional interpolated Cartesian-gridded radar reflectivity values have been partitioned into their stratiform and convective elements, we determine the frequency distribution of radar reflectivity

[10] The sounding-based, monthly mean pressure at the freezing level for February 1988 at Darwin was about 550 hPa, with a standard deviation of ±20 hPa.

[11] The analysis level is not necessarily restricted to a horizontal map of gridded reflectivity. Under some circumstances it may be appropriate to use a Cartesian-gridded low-elevation 360° sweep (PPI) instead.

at each altitude of the three-dimensional data volume. Figure 9 shows the reflectivity frequency distributions for February 1988 at Darwin for two heights (3 and 9 km). The lower altitude is below the 0°C level and represents rain. The distributions are stratified by whether the precipitation was convective or stratiform according to the separation algorithm.

In the rain (Fig. 9a), the distributions of the stratiform and convective radar reflectivity are well separated, by about 15 dBZ. However, the two frequency distributions overlap in the range 20–35 dBZ. This overlap is significant since the rain in this reflectivity range contributes 50% to the monthly total echo area coverage and 46% to the month's rainfall accumulation [estimated by using Eq. (5) of section 10a]. While stratiform rainfall seldom exceeds 10 mm h^{-1} (~35 dBZ), as pointed out by Short et al. (1990) and Rosenfeld et al. (1994), rainfall intensities below that value may be of a convective nature (Fig. 9a). For this reason, and because the reflectivity–rain rate conversion is not unique (see discussion in section 10), *a simple reflectivity threshold method to separate convective from stratiform precipitation is insufficient.*

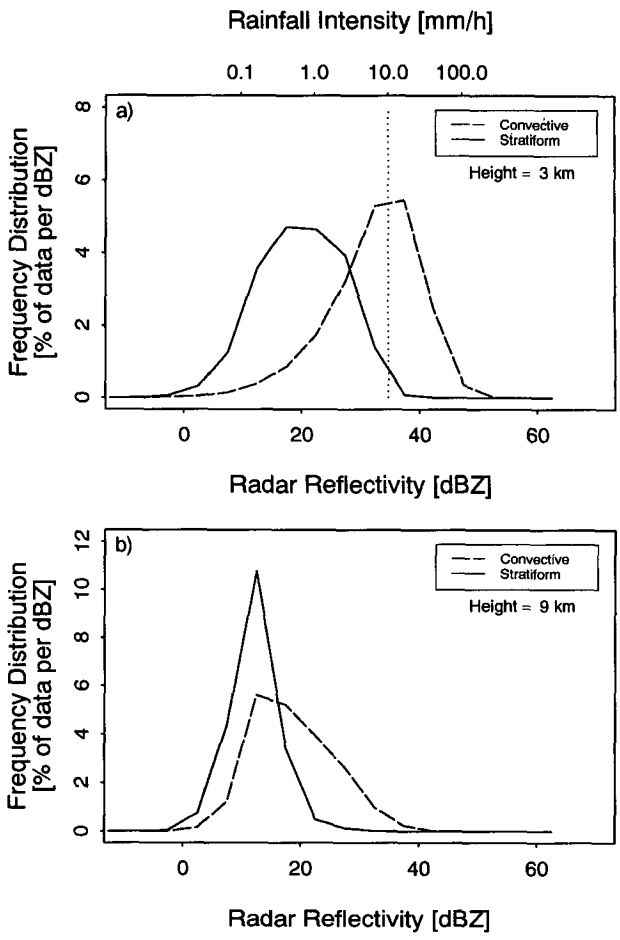

FIG. 9. Frequency distributions of radar reflectivity for February 1988 at Darwin. (a) Convective and stratiform frequency distributions of reflectivity at the 3-km altitude, and (b) convective and stratiform frequency distributions of reflectivity at the 9-km altitude. The vertical dotted line in (a) indicates where a rain-rate threshold of 10 mm h^{-1} would separate convective and stratiform precipitation.

8. Vertical structure

a. *Frequency distribution as a function of altitude—CFAD representation*

The second type of information we extract from the radar data [see item (ii) in section 1] is the vertical structure of the radar echoes. The algorithm we apply to the three-dimensional gridded reflectivity data to summarize vertical structure is simply the frequency distribution of gridded reflectivity values at a given altitude. The frequency distribution of the radar reflectivities observed at higher altitudes is in general different from that at low levels. These statistical differences must be preserved when summarizing the vertical structures exhibited by a large climatological sample of radar echoes.

Figure 9b shows the frequency distributions of convective and stratiform reflectivity at the 9-km altitude for the Darwin February 1988 data. These distributions may be compared to those at the 3-km level (Fig. 9a, section 7). The convective distribution is as wide as at low levels, but shifted toward the stratiform curve. However, the stratiform reflectivities are very narrowly distributed and peak at 10–15 dBZ. Although the stratiform and convective modes at the higher level are much closer than at 3 km, the mean reflectivity values remain about 10 dBZ apart (section 8b).

Frequency distributions of reflectivity can be plotted for altitudes other than 3 and 9 km (Figs. 9a and 9b). Instead of plotting them all separately, however, we display them in a common plot called a "contoured frequency by altitude diagram" (or CFAD; Yuter and Houze 1995b). To indicate how a CFAD is constructed, Fig. 10a shows a frequency distribution of the radar reflectivity values at a given height and time. Similar histograms for all heights at the same time are then plotted and lined up, one behind the other, and shown in perspective view in Fig. 10b. The actual CFAD (Fig. 10c) views the perspective statistical distribution of radar reflectivity with height from the top, by showing the contours of the topography of the perspective diagram.

Figure 11 shows the total, convective, and stratiform CFADs for the Darwin February 1988 data. The total CFAD (Fig. 11a) represents the frequency distribution of reflectivity with height for all data used in this study. The contours in the CFADs show how the frequency distribution varies with height. The CFADs shown in Figs. 11b and 11c represent the ensemble of all the reflectivity volumes centered vertically above the convective and stratiform areas, as identified by the separation algorithm for each single radar volume investigated for February 1988. The distributions in Fig. 9a

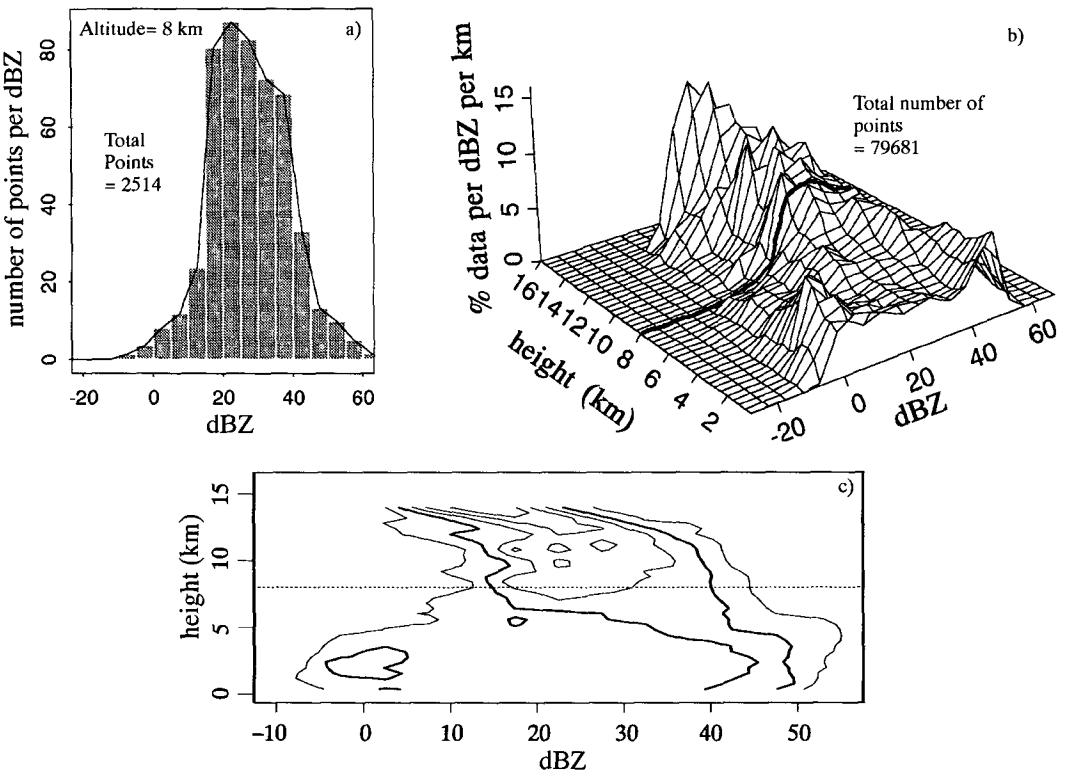

FIG. 10. Statistical presentations of reflectivity data from a three-dimensional volume of radar data collected on 2139 UTC 15 August 1991 during CaPE (Florida). (a) Single-level histogram of radar reflectivity at 8-km altitude. The histogram bin width is 5 dBZ. (b) Perspective view of the frequency by altitude diagram of radar reflectivity obtained by lining up histograms such as the one shown in (a) for all altitudes. The heavy line corresponds to the single-level histogram at 8 km shown in (a). (c) Contoured frequency by altitude diagram (CFAD) of reflectivity, which is a top view of (b). The topography of the frequency distribution of reflectivity is contoured at intervals of 2.5% of data per dBZ per kilometer with the 5% dBZ^{-1} km^{-1} contour highlighted. The horizontal dashed line at 8 km corresponds to the data contained in the single-level histogram shown in (a). (Adapted from Yuter and Houze 1995b.)

and 9b are indicated by the dotted lines at the 3- and 9-km levels.

Yuter and Houze (1995) characterized the transition of convective to stratiform precipitation as depicted in CFADs. They found that radar volume scans taken in stratiform precipitation exhibited narrow reflectivity distributions at all heights, while convection—especially in early stages—showed wider reflectivity distributions. The result of Yuter and Houze was, however, based on a single case. The narrower reflectivity distribution of stratiform precipitation is nonetheless evident in comparing our Fig. 11c with Fig. 11b. Thus, even when all the data for the whole of February 1988 are combined, the CFAD shows a narrower distribution in the stratiform subsample. *As seen previously in a detailed case study, this structure, preserved after extensive data processing and combining data for a whole month, is a further indication that the convective–stratiform separation algorithm is performing well and that the CFAD is a reliable way to represent this structure in a summary fashion.*

b. Vertical profile of mean reflectivity—A monthly bright band

Figure 12 shows the monthly mean vertical reflectivity profiles averaged over the stratiform and convective areas, respectively. The stratiform and convective mean profiles of radar reflectivity exhibit a very similar shape, except for the brightband maximum seen in the stratiform profile at about the 4.5-km altitude. The stratiform profile is almost parallel to the convective profile above the 0°C level. Both profiles show a reflectivity decrease with increasing height of approximately -2.5 dBZ km^{-1} in the range of 5–9 km in altitude (~0°C to −20°C). However, the curves are offset by about 10 dBZ. This reflectivity lapse rate is comparable to the -3.5 dBZ km^{-1} reported by Zipser and Lutz (1994) for continental monsoon break periods at Darwin and the -3 dBZ km^{-1} of New England thunderstorm rainfall found by Donaldson (1961). Those studies, however, were based on median (rather than mean) profiles, and they considered only the cores of maximum reflectivity; that is only the outliers of the reflectivity distribution.

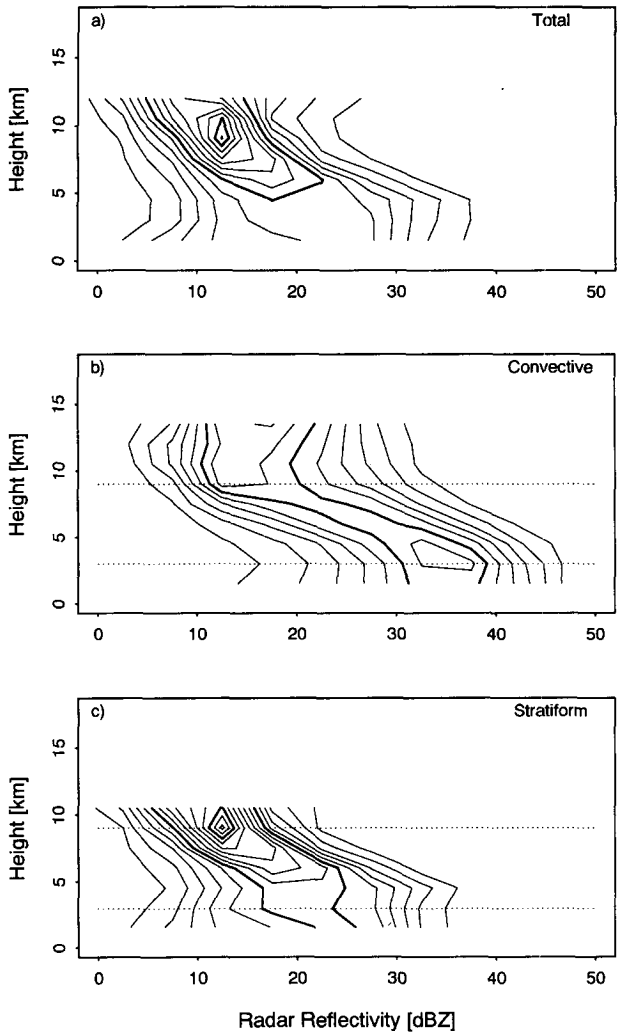

FIG. 11. Climatological contoured frequency by altitude diagrams (CFADs) of radar reflectivity for the volume scans collected at 6-h intervals during February 1988 by the operational radar at Darwin, Australia. CFAD bin size is 5 dBZ. The contours are at intervals of 0.5% of data per dBZ per kilometer, starting with the 0.5% dBZ^{-1} km^{-1} contour. The 3% and 6% dBZ^{-1} km^{-1} contours are highlighted. (a) All radar reflectivity data used in this study, (b) convective radar reflectivity echoes only, and (c) stratiform radar reflectivity echoes only. The dotted horizontal lines in (b) and (c) indicate the altitudes of the reflectivity frequency distributions shown in Fig. 9. The CFADs are truncated at the altitude where the number of points (per height level) drops below 10% of the maximum number of points at any level.

In view of the fact that *an entire month of data,* encompassing a wide variety of precipitation situations, has gone into these mean profiles and that the data have been subjected to several processing steps (interpolation to a Cartesian grid, separation into stratiform and convective components, and averaging over a long time period), *the appearance of the radar bright band in the stratiform profile is yet another indication that the convective–stratiform separation was done properly* and gives us considerable confidence in our algorithm as a whole.

9. Verification of the physical consistency of the convective–stratiform separation—Application to CaPE data

The physical basis for separating convective and stratiform precipitation is the magnitude of the vertical air motion, as discussed in section 6a. Stratiform precipitation occurs where the vertical air motion satisfies (1). Since information about the vertical air motions is generally not available on a routine basis, it is difficult to verify whether our convective–stratiform separation based on radar reflectivity structure actually identifies stratiform and convective regions consistent with the vertical velocity definition.

In this section, we take advantage of an opportunity to verify that our separation algorithm based on radar echo structure is consistent with condition (1). We use a high-resolution dual-Doppler radar dataset collected on 15 August 1991 during the Convection and Precipitation/Electrification Experiment (CaPE) conducted in east-central Florida (Yuter and Houze 1995a). Yuter and Houze analyzed the data on a high-resolution grid (500 m in the horizontal and 400 m in the vertical). The domain covered by the dual-Doppler radar data is about 40 km × 40 km.

We apply our convective–stratiform separation algorithm to two of the dual-Doppler radar volumes collected on 15 August 1991. The separation is done at 2.8-km altitude on a 2-km horizontal resolution gridded reflectivity field, as in case 2d (sections 6c and 6d). Figure 13 shows the radar reflectivity and corresponding convective–stratiform fields for the two volumes investigated. At 2155 UTC, the storm was in a well-developed convective stage, while at 2237 UTC con-

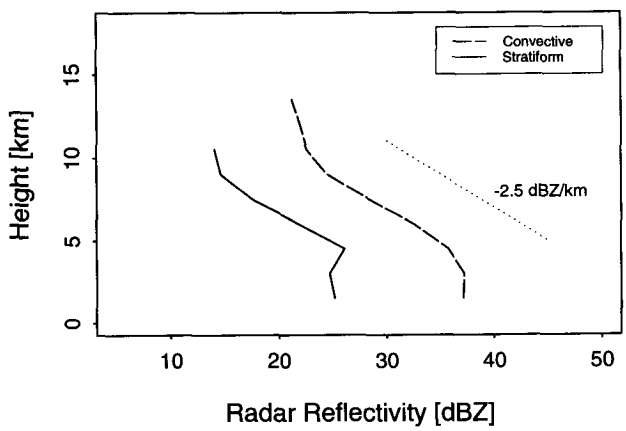

FIG. 12. Mean vertical profiles of radar reflectivity averaged over the areas identified as convective (long-dashed line) and stratiform (solid line) precipitation for February 1988 at Darwin. The profiles are truncated similarly to Fig. 11. The dotted line represents a reflectivity lapse rate of −2.5 dBZ km^{-1}.

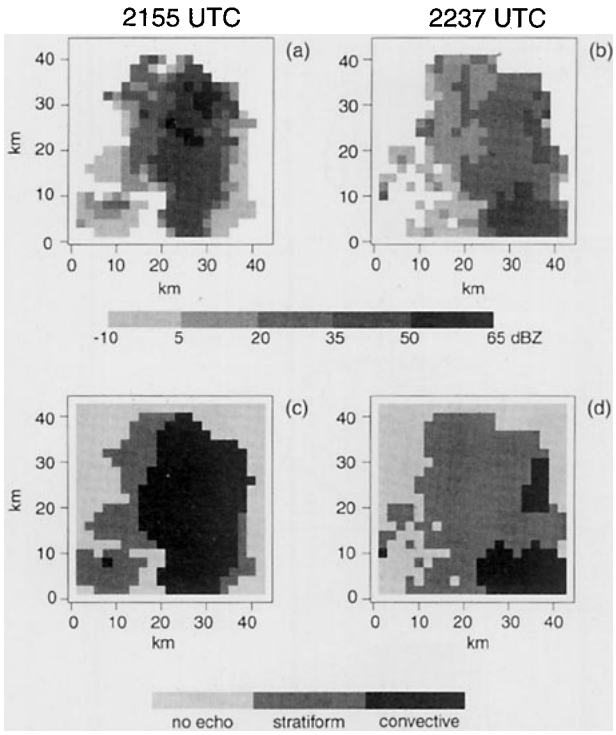

FIG. 13. Horizontal radar reflectivity pattern and objective precipitation classification at 2.8-km altitude for two dual-Doppler radar volumes collected on 15 August 1991 during CaPE. (a) Radar reflectivity pattern at 2155 UTC and (b) reflectivity pattern at 2237 UTC. (c) Convective and stratiform precipitation regions at 2155 UTC and (d) convective and stratiform precipitation regions at 2237 UTC. The horizontal resolution of the data shown in the 40 km × 40 km domain is 2 km.

vection was already decaying and most of the radar echoes in the domain exhibited stratiform rainfall characteristics.

The high-resolution radar reflectivity and vertical air motions for the convective and stratiform regions shown in Fig. 13 were combined and are shown in CFAD format in Fig. 14. The panels to the left show the reflectivity distributions, while the vertical air motions are shown on the right. The top panels illustrate the total CFADs, the center panels represent the convective CFADs, and the bottom panels the stratiform CFADs. These CFADs demonstrate that *the separation of the convective and stratiform precipitation based on the low-level radar reflectivity pattern and using our separation algorithm produces results that are consistent with the physical basis that defines convective and stratiform precipitation.* The vertical air motion distribution of the precipitation areas identified as convective is very wide, exhibiting frequent values larger than ±5 m s^{-1} (Fig. 14d), while the stratiform CFAD is narrower and centered near zero (Fig. 14f). The convective reflectivity distribution (Fig. 14c) peaks at higher intensities and is also much wider than the stratiform (Fig. 14e). The vertical air motions seen in the stratiform areas in general satisfy condition (1). Thus, the convective–stratiform separation applied to reflectivity data (Fig. 13) is verified by vertical velocity data (Fig. 14).

10. Relating radar reflectivity to rainfall intensity

The third type of information we obtain from the radar data [item (iii) in section 1] is the precipitation amount. Several algorithms exist for this purpose. We have experimented with the available techniques, and we now describe the results of these experiments. Before doing so, however, we note two things:

- The separation into convective and stratiform components and the determination of vertical structure of the radar echo field is unaffected by the method used to estimate the low-level rainfall rate. Our stratiform–convective separation and vertical structure methodologies can be combined with any radar rainfall estimation technique.
- All of the available algorithms for converting radar reflectivity Z to rain rate R depend on the combination of the radar data with data from a rain gauge network.

Radar reflectivity is related physically (through Rayleigh scattering theory) to rainfall rate. However, the rain detected by the radar is not identical to the rainfall reaching the earth's surface, since the radar beam is generally well above the surface. In addition, the reflectivity measurements suffer from various beam geometry and range effects (see, e.g., Wilson and Brandes 1979; Zawadzki 1984; Austin 1987; Joss and Waldvogel 1990; Smith 1990). Rain gauges provide a better (though still imperfect) measure of precipitation at the surface—but only at a few points. Radar, on the other hand, provides areal coverage and high spatial resolution. Therefore, the only viable way to measure rain is to combine the radar and rain gauge information. The data from the rain gauge calibrate the radar rain estimates from reflectivity in the vicinity of the gauge. The more rain gauges in a network, the more points can be calibrated in the radar data.

In the tests described below, we find that the way in which a relation between Z and R is formulated is not crucial, as long as some form of rain gauge adjustment is performed.

a. *Single power-law method*

The relation between radar reflectivity Z and rainfall rate R is physically related to the raindrop size distribution. Since both Z and R are different functions of the drop size, this relationship is not unique, though strongly correlated. The Z–R relation is often described by a power law:

$$Z = \alpha R^{\beta}, \qquad (3)$$

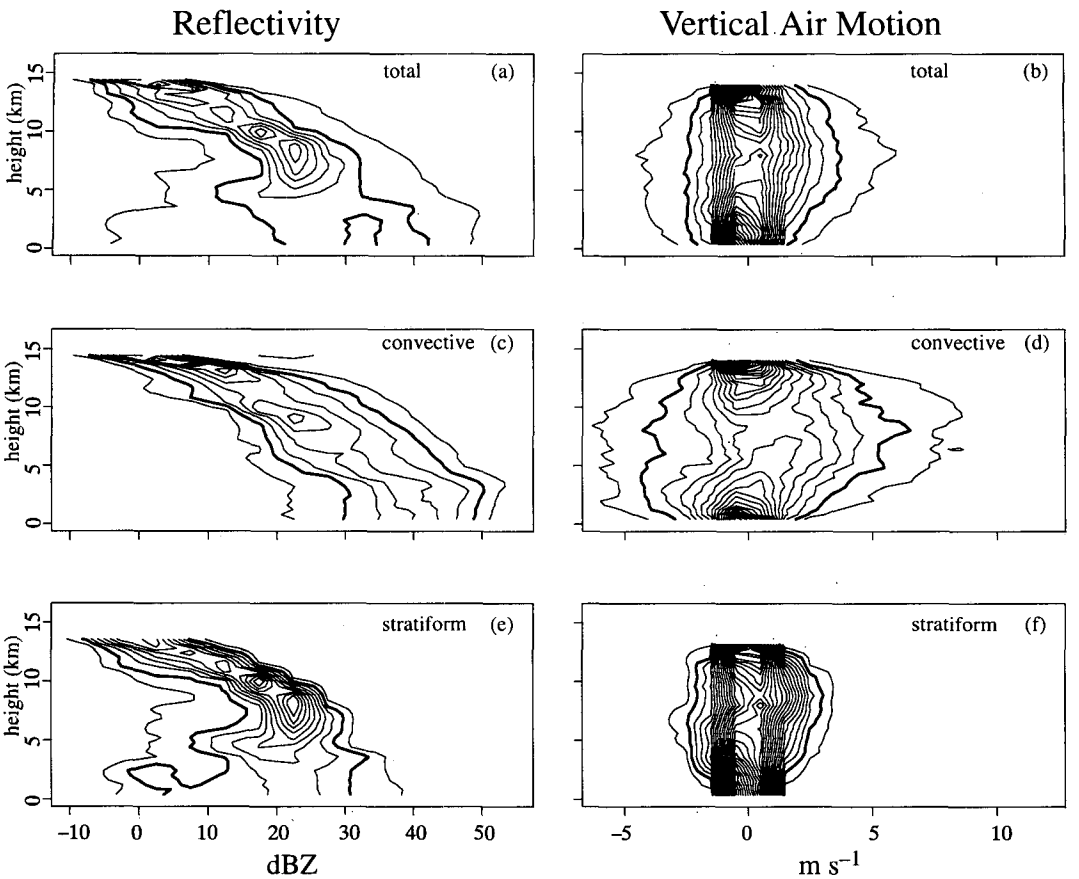

FIG. 14. Contoured frequency by altitude diagrams (CFADs) of radar reflectivity and vertical air motion for the two dual-Doppler radar volumes shown in Fig. 13. Data for both volumes at full resolution (500 m × 500 m × 400 m) are combined in the CFADs. (a) CFAD of reflectivity and (b) CFAD of vertical velocity for all radar echoes in the combined volume. Grid locations within the three-dimensional volumes are classified as either convective or stratiform by their horizontal location using the convective–stratiform maps in Figs. 13c and 13d. (c) and (d) Show the CFADs of reflectivity and vertical velocity for convective regions, and (e) and (f) show the CFADs of reflectivity and vertical velocity for stratiform regions. For reflectivity CFADs, the bin size is 5 dBZ and the plot is contoured at intervals of 2.5% of data per dBZ per kilometer with the 5% dBZ^{-1} km^{-1} contour highlighted. In the vertical velocity CFADs, the bin size is 1 m s^{-1} and the plot is contoured at intervals of 5% of data per meter per second per kilometer with the 10% m^{-1} s km^{-1} contour highlighted.

where Z is the equivalent radar reflectivity factor (mm^6 m^{-3}), R is the rainfall intensity (mm h^{-1}), and α and β are positive numbers determined empirically, usually from measurements of the size spectrum of raindrops in a given precipitation regime. Observations indicate that α varies over a range of a few hundred units (e.g., Battan 1973, 88–97). The factor β, on the other hand, is microphysically limited to the range of $1 \leq \beta \leq 3$ (Smith and Krajewski 1993; Smith 1993). The Z–R relationship most commonly applied to tropical precipitation is

$$Z = 230R^{1.25}. \quad (4)$$

This power-law relation was derived for oceanic tropical precipitation observed during GATE (Austin et al. 1976; Hudlow 1979).

We obtain a rain gauge–adjusted version of (4) by forcing the monthly areal mean rainfall estimated by radar data obtained in the vicinity of rain gauge sites to match the rain gauge–based area-average rain accumulation by using a constant multiplicative correction factor in (4). The continuous rain gauge measurements at the 22 sites around Darwin (Fig. 3, Table 1) approximate the areal mean rainfall for February 1988 as 225 mm. (Note that this average applies only to the gauge sites, not to the entire field of view of the radar, which includes a large oceanic region not covered by rain gauges.)

The radar-based rainfall estimates at each gauge site are obtained from the radar reflectivities for pixels within a circular "window" of specified radius surrounding the rain gauge site (Fig. 15). The radar-based

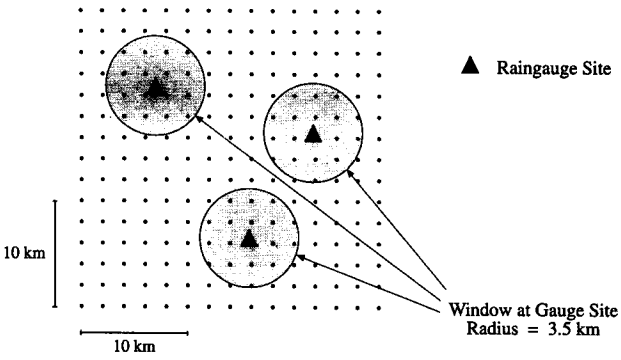

FIG. 15. Schematic diagram indicating how the radar information near the rain gauge sites (triangles) is used for calibration of the radar reflectivity—rainfall intensity conversion. Dots are spaced 2 km apart corresponding to the Cartesian grid resolution of radar data. The shaded circular area around the gauge sites indicates the window of specified radius; only reflectivity pixels within that window are used for estimating the rainfall at a gauge site.

areal mean accumulation is obtained by averaging the radar-based values for all of the gauge sites. The rain gauge adjustment factor for (4) is obtained by dividing the gauge-average accumulation (220 mm)[12] by the radar-based areal mean accumulation at the gauge sites. Table 5 shows the values of the rain gauge adjustment factor obtained for the Darwin February 1988 data for several sets of assumptions regarding the method of how the radar-based rainfall estimates are determined at the rain gauge sites (closest grid point to the gauge, average or maximum within a certain range) and to the specified radius of the window around the gauge. The data in Table 5 indicate that the approach of using the maximum reflectivity value within a certain range of the rain gauge site consistently overestimates the rainfall accumulation and hence does not appear to be a useful method. On the other hand, the radar-correction factor is not very sensitive to the choice of either the average value within a specified range or the closest grid point, as long as the radius around the gauge site is not drawn too large. For a window radius of 3.5 km, these two methods produce a very similar result. These findings are similar to those of Wilson and Brandes (1979) and Klazura (1981).

Based on these tests, we choose a window radius of 3.5 km as the best compromise, which indicates that the radar-based rainfall amounts for February 1988 at Darwin have to be multiplied by a factor of 1.29 to enforce a matching of the areal mean rainfall between the radar estimates at the gauge sites and the rain gauge accumulations. Folding this correction back into the Z–R relationship (4) yields the gauge-adjusted relation

$$Z = 167R^{1.25}. \quad (5)$$

The single power-law approach thus consists of applying this rain gauge–adjusted version of (4) to the radar reflectivity values at each pixel at 3 km (the analysis level for the convective–stratiform separation and surface rainfall estimation), *regardless of whether the reflectivity at that pixel was classified as convective or stratiform.*

While (4) is a general relation based on drop size measurements, (5) is specifically tuned to a particular radar in a particular month and year. It is not generally transferable to data from different months at the same site or to other sites. Equation (4) must be readjusted to obtain a new version of (5) for each month and site to which it is applied. Using the adjusted Z–R relationship (5), we obtain an areal rainfall accumulation averaged over the whole region covered by the radar of 163 mm, roughly 30% less than the 220 mm obtained in the vicinity of the gauges.

Figure 16 demonstrates that when (5) was applied to all the data obtained at Darwin in February 1988, no obvious range dependence appeared in the radar-estimated rainfall or in the ratios of rainfall accumulation estimated by radar and rain gauges. The ratios exhibit increased variability at ranges 90 km and beyond.[13] In the plot, the results for the 1.5-km altitude are also shown, and they also do not indicate a strong range dependence. The lack of strong range dependence could be peculiar to this particular month of data. However, more likely it is because anomalous propagation echoes were edited out of the data (section 5), and the data were objectively analyzed and interpolated to a three-dimensional Cartesian grid so that the precipitation analysis could be performed at a constant

TABLE 5. Sensitivity of the radar–rain gauge adjustment factor to how the radar-based rainfall intensity at the rain gauge site is determined. Equation (4) is used to convert radar reflectivity to rain rate. The radar-based rainfall estimates for the month (at the gauge sites) are compared to the areal mean rainfall accumulation of 220 mm estimated by the Darwin rain gauge network (excluding the Berrimah gauge site) for February 1988 (Table 1).

Method of determining radar-based rainfall estimates at rain gauge site (km)		Radar-based rainfall estimate for month (mm)	Correction factor gauge/radar
Closest grid point		171.5	1.28
Average within	2.0	171.4	1.28
	3.5	170.0	1.29
	5.0	197.9	1.11
Maximum within	2.0	253.4	0.87
	3.5	454.4	0.48
	5.0	680.0	0.32

[12] The rain gauge at Berrimah, the radar site, cannot be used for determining the multiplicative correction factor, since no radar information is available for this gauge site. The areal mean rainfall accumulation for February 1988, based on data of the remaining 21 gauge sites, averages 220 mm (Table 1).

[13] Since the analysis domain is 240 km × 240 km, the radar data beyond a 120-km radius is present only in the corners of the domain.

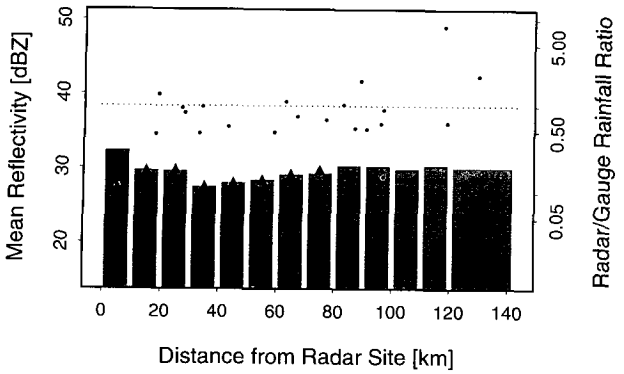

FIG. 16. The azimuthally averaged mean radar reflectivity at the 3-km altitude stratified by range from the radar site is shown by the histogram. The triangles indicate the mean values obtained at 1.5-km altitude. For each rain gauge site, the ratio of the radar-estimated monthly total rainfall at that site and the rain gauge–based continuous accumulation is plotted at the gauge's range from the radar (dots). The horizontal dotted line indicates a ratio of 1. The results are based on the data collected during February 1988 at Darwin, Australia.

altitude, which lies above the ground clutter echo but below the bright band. Significant range effects become dominant sources of error at ranges larger than the ones used in our study (Donaldson 1964; Fabry et al. 1992; Rosenfeld et al. 1992; Kitchen and Jackson 1993).

b. *Separate power laws for stratiform and convective precipitation*

The single power law (5) applies to all the grid points in the radar reflectivity data, regardless of whether the points are classified as convective or stratiform. Joss and Waldvogel (1970) and Joss et al. (1970) showed that the application of different Z–R relations for some distinct precipitation types could improve the accuracy of radar rainfall estimates. Similar results have been reported by Austin (1987). Analyses of raindrop size distribution measurements by Short et al. (1990) indicate that convective and stratiform rainfall of tropical squall line precipitation systems of the type that often occur in the Darwin area exhibit characteristic raindrop spectra resulting in two different radar reflectivity–rainfall intensity relationships. The Z–R relation given by Short et al. (1990) for the convective rainfall is

$$Z = 170R^{1.47}. \quad (6)$$

Though Short et al. do not give a relation for the stratiform part of the rainfall, it appears from their Fig. 7 that the relationship of Joss et al. (1968) and Joss and Waldvogel (1970):

$$Z = 300R^{1.5} \quad (7)$$

closely represents the disdrometer-based observations of the stratiform raindrop spectra at Darwin.

These Z–R relationships, which are based on raindrop spectra observations, are rain gauge adjusted following a procedure similar to that used to obtain (5). We force the areal mean radar rainfall estimate at the rain gauge sites to match the gauge-based areal mean rainfall accumulation. Instead of applying a single Z–R relation to each radar pixel, however, (6) and (7) are used to convert convective and stratiform radar echoes to rain rate. Since the ratio between the multiplicative factor for convective [α_c = 170, Eq. (6)] and stratiform [α_s = 300, Eq. (7)] rain is climatologically determined, we apply a single adjustment factor to preserve this ratio. Folding the derived correction factor of 1.64 back into the stratiform and convective Z–R relationships, we obtain the rain gauge–adjusted versions of (6) and (7):

$$Z = 82R^{1.47} \quad \text{for convective rain} \quad (8)$$

$$Z = 143R^{1.5} \quad \text{for stratiform rain.} \quad (9)$$

The rainfall map for the month and the map of the distribution of the convective rainfall fraction obtained by (8) and (9) are nearly indistinguishable by eye from those obtained from simply applying (5) to all the echoes. Table 6 lists the estimates of the total February 1988 mean rainfall over the entire area covered by the Darwin radar. The February 1988 areal rainfall obtained using (8) and (9) to convert convective and stratiform radar reflectivity to rainfall intensity is 162 mm, almost identical to the value obtained with the single power-law approach (163 mm). The third value in the table is obtained by the probability matching method, to be discussed below.

c. *Probability-matching method*

Instead of using Z–R relationships based on measurements of drop size spectra [e.g., (4) or (6) and

TABLE 6. Areal rainfall estimates for February 1988 at Darwin, Australia. The various rainfall accumulations are estimated using three different methods to convert radar reflectivity to rainfall rate. The convective contribution to the rain volume is given for the total areal rainfall and separated between rain that fell over land and ocean.

Z–R conversion	Monthly areal rainfall (mm)	Convective rainfall fraction			
		Total	Land	Ocean	Ratio land/ocean
Single power law	163.2	58.6%	35.7%	22.9%	1.56
Double power law	162.4	59.8%	36.4%	23.4%	1.55
Probability matching	170.5	65.5%	39.9%	25.6%	1.56

(7)], Miller (1972) and Calheiros and Zawadzki (1987) proposed deriving the Z–R relation directly from radar and rain gauge measurements. They matched equal percentiles of the probability density functions of the radar-derived reflectivities Z and the gauge-derived rain rates R. This technique is called "probability matching" and has the advantage that many of the problems associated with measuring reflectivity are incorporated into the relationship since the resulting Z–R is based on the actual radar measurements rather than the theoretical reflectivity based on drop size measurements (Atlas et al. 1990b; Rosenfeld et al. 1993).

In fact, the probability-matching method is another form of rain gauge adjustment. By matching the frequency distributions of radar and rain gauge measurements, the Z–R relation derived by probability matching, when applied to the radar data, is forced to give rainfall accumulations consistent with the gauges. The essential difference from the rain gauge adjustment described above (sections 10a and 10b) and probability matching is that in the latter the frequency distributions of the radar and rain gauge data are matched percentile by percentile, while in the methodology described above only the means of the distributions are forced to match.

The probability-matching method would appear to be more elegant; however, it also has the disadvantage that it requires a large and homogeneous sample of simultaneous radar and (high-resolution recording) rain gauge data to produce a stable relationship (Krajewski and Smith 1991; Rosenfeld et al. 1993). Range effects, life cycle stages, scale differences (local isolated thunderstorm versus larger mesoscale convective systems), and local climatological effects (e.g., ocean, continent, large island, small island, coastal influences, hills, mountains) must all be taken into account. This requirement leads to much subdivision and grouping of the data into various categories, which in turn require the length of record used to obtain a statistically significant sample to be quite large. A month of data at a site like Darwin, which has continent, ocean, island, and coastal influences as well as monsoonal and break regimes appears marginal for application of probability matching in its original form (Rosenfeld et al. 1993).

The development of the "window probability-matching method" (WPMM; Rosenfeld et al. 1994) relates the frequency distribution of reflectivity obtained only from radar data taken within small spatial windows at the gauge sites with the rain gauge–based frequency distribution of rainfall rates taken within small time windows around the radar sampling times. This method relaxes some of the previous constraints regarding the homogeneity of precipitation. Because of the reduced sample size, however, the minimum length of measurement period to acquire a stable Z–R relation increases for a particular type of precipitation.

To compare the behavior of a Z–R relation based on probability matching to the rain gauge–adjusted single and double power-law relationships described above, we use a WPMM Z–R relation determined by Rosenfeld et al. (1994) for Darwin. We do not derive our own probability-matched Z–R since our study is based only on four radar volumes per day, which would not give us a large enough sample to obtain a stable relationship. We use the WPMM Z–R determined for the special observation period (SOP) 87/3 at Darwin (27 January 1988–17 February 1988) that is closest to the February 1988 data used in this study (see Fig. 8c of Rosenfeld et al. 1994). Application of this SOP Z–R relation to the February 1988 data results in a radar rainfall estimate of 165 mm at the rain gauge sites, which is significantly lower than the gauge accumulation of 220 mm. This difference may be a consequence of the mismatch in time periods. A minor adjustment of -1.5 dBZ to Rosenfeld's WPMM Z–R, however, produces a very close agreement between the radar-rainfall estimate at the gauge sites and the rain gauge total. *Therefore, we have adapted the characteristic shape of the window probability-matched Z–R and applied a small gauge adjustment similar to the ones discussed previously.* It is this February 1988 gauge-adjusted WPMM relation that is used hereafter.

The areal mean rainfall, averaged over the whole region covered by the Darwin radar and using this probability-matched Z–R relation to convert reflectivity to rainfall rate—independent of whether the precipitation has been classified as convective or stratiform—totals 170 mm for February 1988, which is very close to the values obtained by either using a single or double power law Z–R approach (Table 6).

d. Rain area method

The power-law method(s) and the probability-matching technique described above are two ways to obtain pixel-by-pixel values of rainfall rate from measurements of reflectivity. If only the area-integrated rain amount is desired rather than point values of rain rate, then an alternative method can be used, for example, the area–time integral (ATI) or area-threshold method (e.g., Doneaud et al. 1981, 1984; Chiu 1988; López et al. 1989; Kedem et al. 1990; Atlas et al. 1990a; Krajewski et al. 1992; Cheng and Brown 1993) or the height–area threshold (HART) method (Rosenfeld et al. 1990). However, we use high-spatial-resolution rain-rate maps as one of the building blocks of our monthly rainfall climatology. Testing of these rain-area methods on the February 1988 data is outside the scope of this study.

11. Further analysis of the data of Darwin, February 1988: Area covered by radar echo, area-integrated rainfall, and land–ocean differences

a. Cumulative distributions as a function of radar echo intensity

In this section, we use the gauge-adjusted single power-law method (section 10a) to illustrate various ways of summarizing the rainfall of February 1988 near Darwin. Figure 17 shows the relative contributions of the radar echoes exceeding a certain reflectivity threshold to the total echo-covered area and the total rain volume for the month. About 95% of the rain resulted from radar echoes with $Z \geq 20$ dBZ. However, these echoes only covered about 55% of the total rain area. Rain with $Z > 30$ dBZ contributed 70% to the monthly rain volume but only 15% of the area covered by rain. These characteristics are typical of tropical rainfall (e.g., Rosenfeld et al. 1990) and suggest that the February 1988 data obtained at Darwin are fairly representative of tropical conditions.

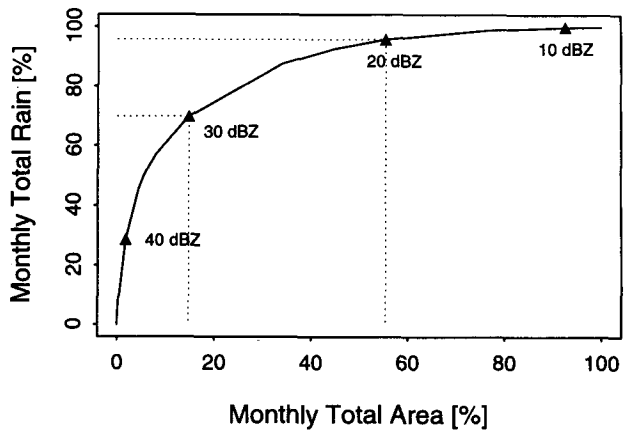

FIG. 17. Relative contributions of the radar echoes exceeding a certain reflectivity threshold to the total echo-covered area and the total rain volume for the February 1988 data collected at Darwin, Australia.

b. Area covered by echo as a function of how widespread the precipitation was

We determined the fraction of the radar-observed domain covered by precipitation echo for each individual radar volume analyzed. The number of times that a given fractional echo area coverage was observed is given by the number printed at the top of each bar in Fig. 18a. The smallest area coverage ($\leq$3.5%, excluding no-echo cases) was seen most frequently (44 times). The largest areal coverage, observed only once, was 63%. The height of each bar in the graph shows the net area covered by all the individual volumes in that category combined and normalized to the monthly total. Even though the volume with largest areal coverage occurred only once, it comprised more total echo area than the 44 volumes with smallest echo coverage. Cumulative distributions for number and area are also shown in Fig. 18a. They indicate that 10% of the radar volumes exhibiting the most extensive area coverages account for about 50% of the monthly total echo area coverage. This behavior is typical of tropical precipitation (López 1976; Houze and Cheng 1977; Houze and Betts 1981).

c. Area covered by echo according to whether it was stratiform or convective

Figure 18a is replotted in Fig. 18b; however, now each bar is subdivided. The lighter-shaded portion of the bar shows the contribution of stratiform precipitation to the total echo-covered area, while the darker portion shows the contribution of convective precipitation to the total. Cumulative distributions are shown for both stratiform and convective precipitation. They show that 88% of the total area covered by precipitation radar echoes during February 1988 at Darwin was stratiform, while convective elements contributed only 12%. The convective contribution decreases with increasing total area covered by precipitation. This characteristic reflects the fact that situations in which a large fraction of the observational area is covered by precipitation are dominated by mesoscale convective systems with large regions of stratiform precipitation.

d. Total rainfall as a function of how widespread the precipitation was

Figure 19a is the same as Fig. 18a, except now each bar represents the total amount of rain instead of the net area covered by radar echo. To obtain Fig. 19a, the radar reflectivity Z in each of the echo volumes was converted to rainfall rate R, and the total rain amount was obtained by integrating the resulting field of R with respect to area. The single power-law Z–R method [section 10a, Eq. (5)] was used to convert reflectivity to rain rate. The many (44) cases of relatively isolated rain areas take on more importance when weighted by rain rate (compare the bar graphs in Figs. 18a and 19a) since those cases include isolated, but intense convective showers—that is, hectors. Nonetheless, the cases of large areal coverage (right-hand bars in Fig. 19a) still account for large total rain amounts even though they do not occur frequently. The cumulative distributions shown in Fig. 19a show that the same top 10% of the domain coverage observations (Figs. 18a and 19a, dotted line) that contributed 50% to the monthly total echo area coverage (Fig. 18a, dashed line) accounted for about 70% of the monthly total rainfall (Fig. 19a, dashed line), again consistent with previous studies of tropical precipitation (Houze and Betts 1981).

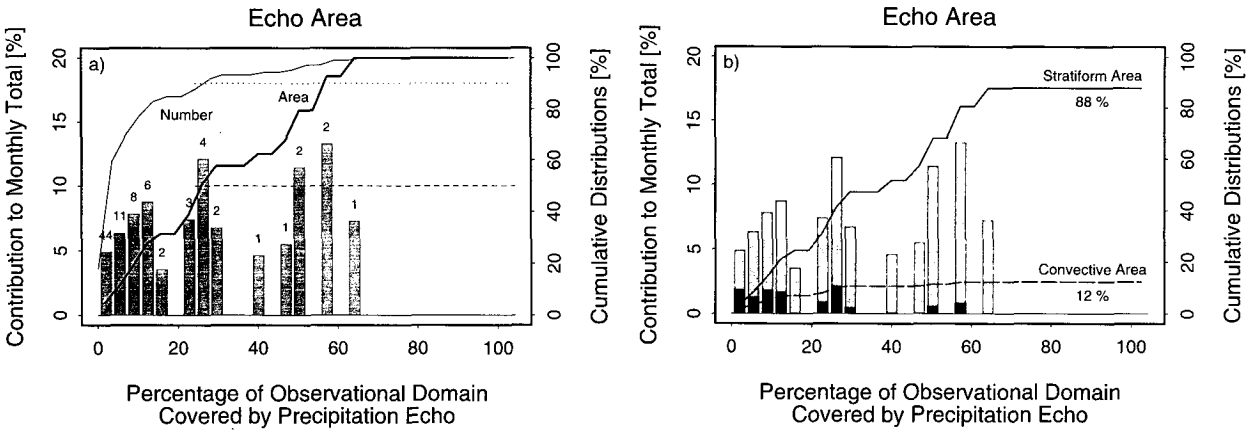

FIG. 18. (a) Histogram of contribution to monthly total echo area coverage as a function of instantaneous percentage coverage of the observational domain (Fig. 3). The numbers on top of the bars indicate the number of samples (radar volumes) in each size class. The cumulative distribution curves of the number (thin line) and area size (heavy line) are shown. At 90% cumulative number of samples (dotted line), the corresponding cumulative area is 50% (dashed line). (b) Histogram of relative contributions of convective (dark shaded) and stratiform (light shaded) precipitation echoes to the monthly total echo area coverage as a function of echo area coverage. The cumulative fractions and their overall contribution to the monthly total are shown by the long-dashed (convective) and solid (stratiform) lines.

e. Total rainfall according to whether it was stratiform or convective

Figure 19b is in the same format as Fig. 18b, except that it portrays the total rainfall rather than the area covered by radar echo; the dark shading of the bars indicates the convective and the light shading the stratiform contribution. The bars in Fig. 19b show that largest amounts of stratiform precipitation occurred on days when the area surveyed by the radar was more widely covered by precipitation. On those days, large mesoscale convective systems with large stratiform regions accompanying the convection were responsible for the rainfall. The cumulative distributions in Fig. 19b show that the overall contributions to the monthly accumulation by stratiform (41%) and convective (59%) precipitation are similar to those found previously for tropical, oceanic and continental convection (e.g., Houze 1977; Cheng and Houze 1979; Gamache and Houze 1983; Leary 1984; Churchill and Houze 1984; Houze and Rappaport 1984; Wei and Houze 1987; Chong and Hauser 1989; Gage et al. 1994).

Using the double power law (Fig. 20a) or the probability-matching Z–R approach (Fig. 20b) instead of the single power-law relation, we obtain results very similar to those obtained with the single power law (Fig. 19b). The probability-matching approach revealed a slightly larger convective rainfall fraction (66% compared to 59% with the single power law), as shown in Table 6. However, the three different techniques investigated to convert radar reflectivity to rain rate produced convective contributions to the monthly rainfall accumulation within 7% of each other.

Rosenfeld et al. (1995) found convective rainfall contributions of 80% and more for precipitation in the vicinity of Darwin. However, their results are heavily based on rain gauge data, which, being over land, sampled the more convective land and island rainfall, whereas the 59:41 ratio we obtain includes both ocean and land rainfall. Moreover, their study included different time periods than ours, and they use a stratiform–convective separation technique that probably underestimates the stratiform amount (section 6b).

f. Land–ocean differences

The monthly areal rainfall accumulation for February 1988 was estimated at 163 mm (Table 6) for the entire radar-covered area with the single power-law Z–R relation. This is about 30% less than estimated by the land-based rain gauge network. Since the radar estimates are gauge-adjusted such that the radar data in the vicinity of the rain gauges match the gauge totals (section 10a), the rain accumulation over land appears to have been greater than that over water. Though the areas covered by land and ocean of the studied domain are comparable in size, 60% of the monthly total rainfall (and area coverage) was over land, while 40% was over ocean.

The monthly mean vertical precipitation characteristics (mean profile of radar reflectivity and CFAD), both subdivided into convective and stratiform precipitation, are found to be very similar over land and over ocean for February 1988. The mean reflectivity profiles over land and ocean are barely different from Fig. 12, and the CFADs separated by land and ocean are indistinguishable from Fig. 11. The monthly mean rainfall rate averaged approximately 14 mm h^{-1} for the convective precipitation areas, while the stratiform counterpart was only about 1 mm h^{-1} over both land and ocean. The fraction of the rain area covered by convective echoes over land and ocean was 7% and 5%

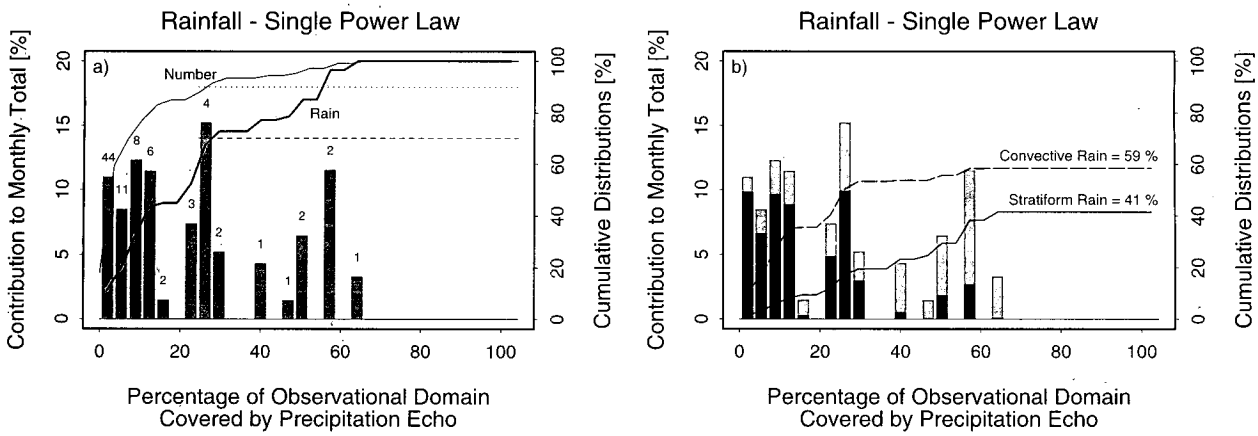

FIG. 19. (a) Histogram of contribution to monthly total rainfall as a function of instantaneous percentage coverage of the observational domain (Fig. 3). The numbers on top of the bars indicate the number of samples (radar volumes) in each size class. The cumulative distribution curves of the number (thin line) and rain volume (heavy line) are shown. At 90% cumulative number of samples (dotted line), the corresponding cumulative rainfall is 70% (dashed line). (b) Histogram of relative contributions of convective (dark shaded) and stratiform (light shaded) precipitation echoes to the monthly total rain volume as a function of echo area coverage. The cumulative fractions and their overall contribution to the monthly total are shown by the long-dashed (convective) and solid (stratiform) lines. The gauge-adjusted single power-law Z–R relation [section 10a, Eq. (5)] is used to convert radar reflectivity to rainfall rate.

of the monthly total, respectively, and the convective contribution to the rain volume was 36% over land and 23% over ocean (Table 6). The ratio of about 3:2 between the rainfall accumulations over land and over ocean was thus mainly determined by the different convective contributions to the radar echo area coverage and the rain volume. The higher convective contribution over land was mainly associated with hectors.

The land–ocean differences in rainfall discussed above are not dependent on the choice of Z–R relationship to convert radar reflectivity to rain rate. The ratio of the monthly convective rainfall fraction over land and ocean remains 3:2 whether the single power-law, double power-law, or probability-matching Z–R conversion is used (Table 6).

g. *Spatial variability of monthly rainfall and its convective fraction*

The spatial distribution of the monthly rainfall accumulation for February 1988 and the convective contributions to the monthly total at each individual point within the area 240 km × 240 km are shown by Figs. 21a and 21b, respectively.[14] Figure 21a provides a visual confirmation of the fact that more rain fell over land than over ocean (section 11f). The largest rainfall accumulations occurred over Bathurst and Melville is-

[14] Note that a significant part of the spatial variability seen in these rainfall maps has to be attributed to the limited number of samples used to derive them.

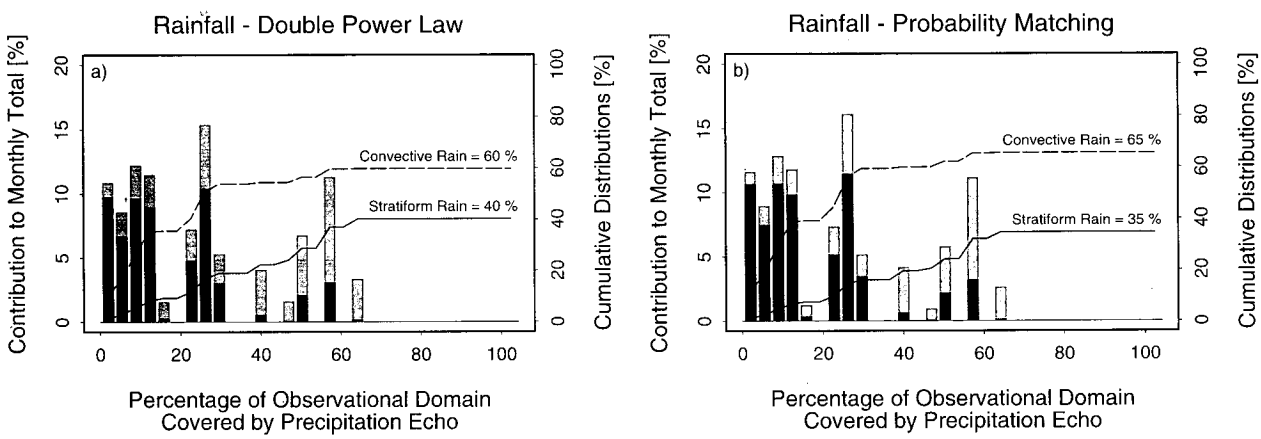

FIG. 20. Similar to Fig. 19b, but using different Z–R approaches. (a) Gauge-adjusted double power-law Z–R relations [section 10b, Eqs. (8) and (9)]. (b) Window probability-matching Z–R relation (see section 10c).

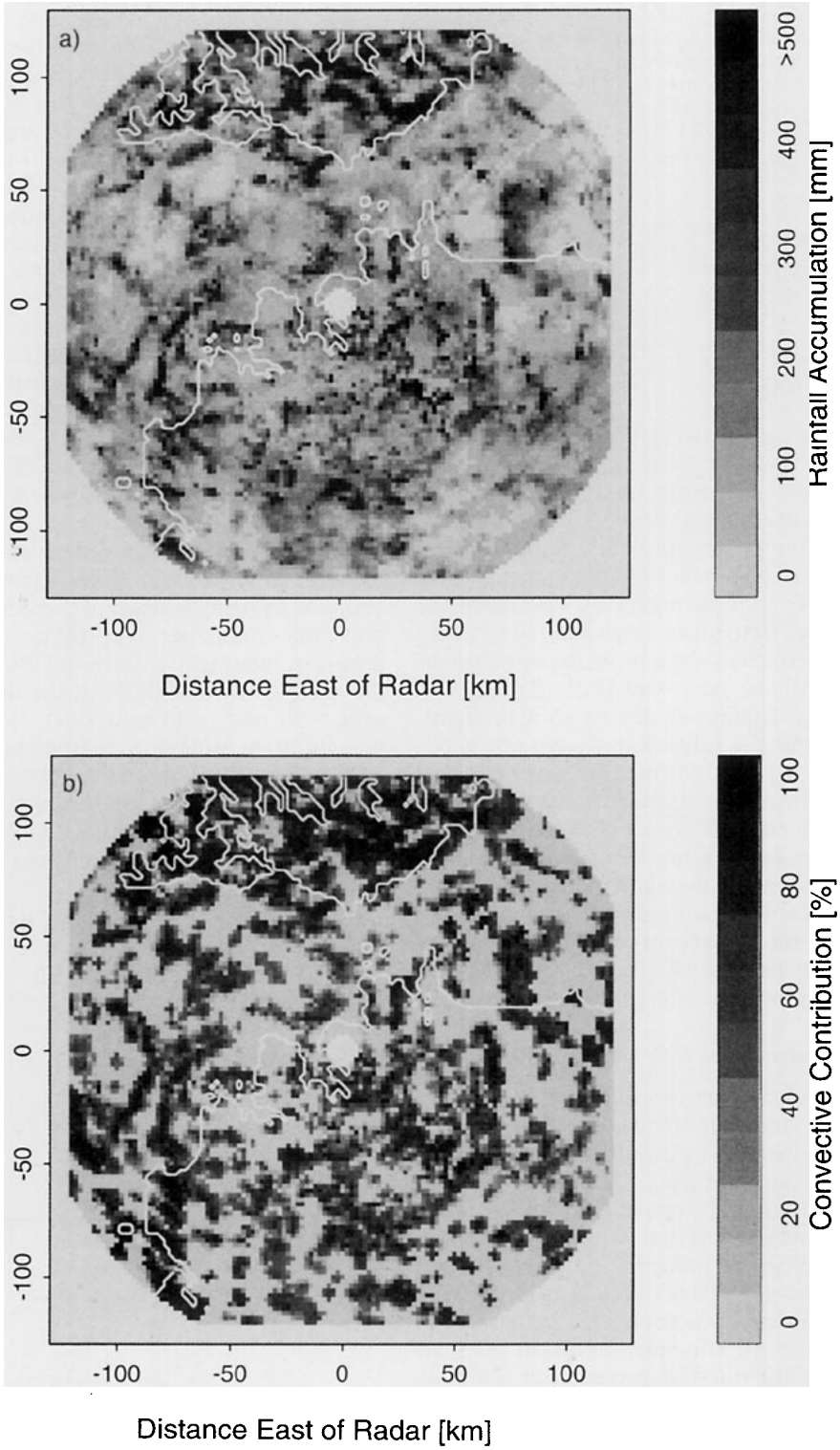

FIG. 21. (a) Spatial distribution of the monthly rainfall accumulation for February 1988 based on the radar volume scans taken at 6-h intervals and using a rain gauge–adjusted GATE Z–R relationship [section 10a, Eq. (5)]. (b) Spatial distribution of the convective contribution to the monthly rainfall accumulation at each point of the domain. The geographical map is indicated by the white contours.

TABLE 7. Differences in the spatial distribution of rainfall and convective rain fraction obtained by subtracting maps of monthly rainfall accumulation computed by different Z–R relations. The three different methods are the single power law (SPL), double power law (DPL), and window probability matching (WPMM).

Difference between Z–R methods method 1 − method 2	Root-mean-square difference: Rainfall accumulation (mm)	Root-mean-square difference: Convective fraction
SPL − DPL	27.5	2.9%
SPL − WPMM	49.7	4.5%
DPL − WPMM	40.7	4.9%

lands north of Darwin in association with the heavily convective hector thunderstorms, which is also indicated by the highly convective contribution to the rainfall total over the islands (Fig. 21b).

To determine the sensitivity of the monthly areal rainfall distribution to the method used for conversion of radar reflectivity to rainfall rate, we compared the monthly rainfall accumulation maps and the monthly convective rainfall fraction maps using the single power law (Fig. 21), the double power law [Eqs. (8) and (9)], and the window probability-matching Z–R methods. Table 7 summarizes the root-mean-square (rms) differences between the different methods for each type of map. Consistent with the statistics for monthly areal rainfall (Table 6), the differences between the single and double power-law approaches are smaller than those comparing either power-law method to probability matching (Table 7). Although the rms difference of rain accumulation in the point-to-point comparison between maps may be up to 50 mm, the rms difference in monthly convective rainfall fraction is less than 5%.

12. Uncertainty associated with sampling frequency

If algorithms for convective–stratiform separation, vertical structure, and rain amount are to be applied to extract climatologically relevant information from operational radar and rain gauge data, we must optimize the data sampling. The rate of data flow from the operational sites may exceed that required for building a reliable climatology of precipitation structure and amount. In this study, we have sampled at a frequency of 6 h. With automated procedures for ingesting and editing data, we can, in principle, sample at intervals of about 10 min. The question arises: what sampling interval is *required* for a reliable climatology? In this section, we address this question in regard to the monthly areal mean rainfall by means of rain gauge records.

a. Darwin, February 1988

The basic block of information is the 15-min rainfall accumulation (mm) at a rain gauge site. With 96 15-min samples per day and 29 days in February 1988, we have 2784 blocks of information at each of the gauge sites listed in Table 1. From these blocks of information, any sampling scenario can be simulated by extracting a subset of blocks and using only those blocks to estimate the mean rain rate for the month. We express the selected 15-min sample as an hourly rain rate (mm h^{-1}). Each 15-min rain rate is assumed to be representative of the entire time period between samples. The rainfall accumulation for the month at each gauge site is obtained by multiplying the monthly mean rain rate by 696 h (the total number of hours in February 1988). The values obtained at the 22 rain gauge sites are then averaged to estimate the areal mean rainfall accumulation for the month.

The most accurate estimate is obtained by using every 15-min sample at each site. The areal mean accumulation obtained in this way for February 1988 is 225 mm (section 10a, Table 1). If we use a subset of the samples, we obtain a different value. To illustrate the variability of the possible estimates that could be obtained by using a subset of the samples, we may take only one sample per day—always taken at the same time (e.g., midnight). We repeat this calculation taking the sample at other times of the day (midnight +15 min, +30 min, +45 min, etc.). We thus obtain the mean diurnal rainfall cycle (over land) in the vicinity of Darwin for this particular month (Fig. 22). The mean rainfall is minimum during the morning (0800–1300 LST) and maximum, with a double peak, in the afternoon. The first peak is due to the hectors over the

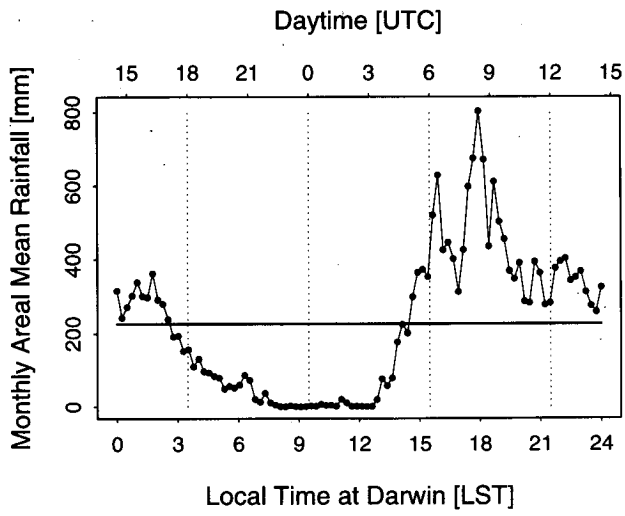

FIG. 22. Rain gauge–based monthly areal mean rainfall accumulation estimated from one 15-min sample per day, as a function of the time of day the sample is taken (solid line with dots). This figure reflects the monthly area-average diurnal rainfall cycle over land for February 1988 at Darwin. The heavy horizontal line indicates the true monthly areal mean rainfall accumulation for this particular month and site based on the continuous rain gauge record. The dotted vertical lines indicate the sampling times of the radar volume scans investigated in this study.

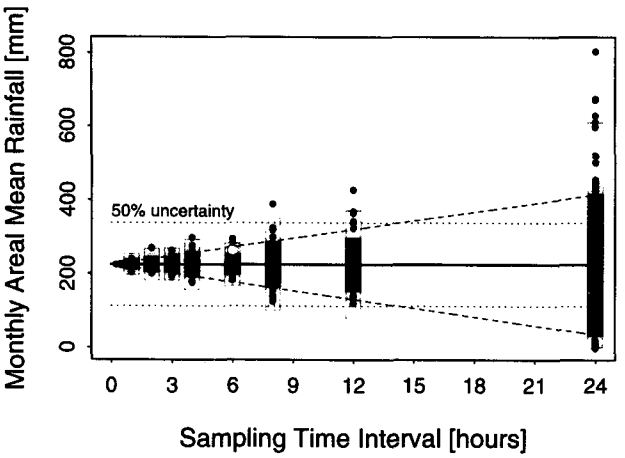

FIG. 23. Uncertainty of monthly areal rainfall estimates as a function of the sampling time resolution. The results are based on the Darwin rain gauge network data of February 1988 and a sampling scenario as explained in the text. The dark (light) shaded area in each sampling time interval bin corresponds to the range of the mean plus/minus one (two) standard deviation(s). The open (white) circle within the 6-h sampling interval bar indicates the result based on the rain gauge data at the radar sampling times used in this study (264 mm). The heavy horizontal line indicates the true monthly areal mean rainfall accumulation for this particular month and site based on the continuous rain gauge record (225 mm). The 50% uncertainty range is shown by the dotted horizontal lines. The sloping dashed lines indicate that decreasing the sampling time resolution increases the uncertainty of the monthly areal rainfall estimate by roughly 3.5% per hour decrease in time resolution.

islands north of Darwin (Keenan et al. 1990). Qualitative inspection of Fig. 22 suggests that sampling at 6-h intervals, as we have done in this study, only barely takes into account the diurnal cycle (dotted lines in Fig. 22).

To obtain an estimate of the uncertainty associated with the sampling time interval, various sampling frequencies have been examined. All the different estimates based on taking only one sample per day, as discussed above, result in the range of values plotted at the sampling time interval of 24 h in Fig. 23. Increasing the sampling frequency from one to two samples per day, we obtain the range of values plotted at the sampling time interval of 12 h in Fig. 23. These estimates of monthly rainfall range from 120 to 430 mm, depending on what time of day the samples are taken. The sampling interval is then reduced to 8 h, and the points plotted at 8 h in Fig. 23 are obtained. The spread of estimates is reduced somewhat to about 125–390 mm. Further reduction of the spread is seen in Fig. 23 as the sampling interval is successively reduced. For a sampling interval of 1 h, the spread is from 205 to 240 mm, only slightly deviating from the true mean of 225 mm (Table 1)—that is, all the estimates calculated with 1-h sampling produce a monthly areal rainfall estimate within about 10% of the true accumulation.

The scatter of the points in Fig. 23 measures the uncertainty of any estimate obtained with a given sampling time resolution. The dark (light) shaded area at each sampling time represents the range of one (two) standard deviation(s) from the mean based on all the data (225 mm, Table 1). The sloping dashed lines approximately enclose the estimates that are within one standard deviation of the mean accumulation. *The slopes of these lines indicate that the uncertainty of the monthly areal mean rainfall estimate, expressed as the standard deviation of estimates based on all the possible regularly spaced sampling intervals, increases roughly 3.5% per hour increase in sampling time interval.* On the average, at least eight samples per day would be necessary to estimate the monthly areal mean rainfall accumulation within 10% accuracy. This result agrees with Seed and Austin (1990), who found that about 8–16 samples were required to meet the 10% accuracy limit for comparable area sizes in Florida. Figure 23 suggests that the accuracy of our monthly areal rainfall analysis (163 mm, Table 6), which is based on a 6-h time resolution, is about 15%–20%.

b. *Other months of data from the same and a different rainy season*

To broaden the basis of the analysis regarding the uncertainty of the monthly areal mean rainfall estimate as a function of the sampling frequency, other months of data collected at Darwin, Australia, have been analyzed. A total of eight months of rain gauge data from two different rainy seasons have been investigated. Despite interannual and seasonal variations, the sampling uncertainty remains about the same (Table 8). The uncertainty of the monthly areal mean rainfall accumulation was always found to increase by about 3%–4% per hour increase in sampling time interval. These results imply that for Darwin, Australia, precipitation has to be sampled once every hour if the uncertainty of the monthly areal mean rainfall accumulation has to be less than 10%. However, a sampling time reso-

TABLE 8. Uncertainties as a function of sampling frequency based on tipping bucket rain gauge data over two rainy seasons at Darwin, Australia. The last column expresses the increase of uncertainty of the estimated monthly areal mean rainfall per hour decrease in sampling time resolution.

Month	Year	Number of gauges	Monthly areal mean rainfall (mm)	Uncertainty increase (% h^{-1})
December	1987	22	378	2.5
January	1988	22	194	3.5
February	1988	22	225	3.5
March	1988	22	255	3.0
December	1989	22	158	4.5
January	1990	24	336	2.5
February	1990	24	171	4.0
March	1990	21	213	3.0

lution of 3 h may, in the average, produce monthly areal rainfall estimates with an accuracy of approximately ±10%.

These results are valid for Darwin and a domain size corresponding to the area represented by the rain gauge network. Assuming that for monthly rainfall accumulations the gauge network represents roughly half the area (land only) covered by the Darwin radar umbrella out to a range of about 125 km (Fig. 3), the sampling uncertainty statistics presented above are valid for a 1.5° latitude–longitude box. Using the space-scaling behavior discussed by Bell et al. (1990), for example, our results are in agreement with sampling uncertainty studies presented for the TRMM satellite and monthly rainfall estimates over a 500 km × 500 km domain (see Simpson 1988, 36–41).

13. Conclusions

The methodology presented in this paper processes the data stream from operational radar and rain gauge networks to obtain climatological information that

(i) distinguishes between convective and stratiform precipitation,
(ii) statistically represents the vertical structure of radar echoes, and
(iii) determines precipitation amount.

The algorithms used to obtain this information are simple, easy to apply to large operational datasets, and can be used either separately or in combination with each other.

The particular algorithm we use for distinguishing between convective and stratiform precipitation is based on the intensity and sharpness of maxima in horizontal patterns of reflectivity. It is the latest refinement of a technique initiated by Houze (1973) and further developed by Churchill and Houze (1984) and Steiner and Houze (1993). This algorithm has several advantages. Most importantly, it divides convective and stratiform precipitation according to the physical definition of stratiform precipitation (section 6a). Independent data on vertical air motions in a region containing both convective and stratiform precipitation verify that the physical definition is satisfied when our algorithm is applied to radar reflectivity data (section 9).

In addition to being physically consistent, our convective–stratiform separation algorithm has the following practical advantages:

- By finding first the convective precipitation and defining the remainder as stratiform, we allow for the possibility that the stratiform precipitation might not exhibit a bright band because of its age, its juxtaposition relative to convective precipitation areas, or its distance from the radar site.
- By identifying convective cores in horizontal precipitation echo patterns, we take advantage of the fact that strong convective echo cores can be seen in horizontal radar echo patterns out to much farther range than is possible to resolve a bright band in vertical cross sections. We thus gain area coverage, out to the maximum range for which the radar can estimate rainfall.
- The same criteria to divide the precipitation into stratiform and convective components are applied throughout the field of view of the radar. By applying the algorithm uniformly across the domain, no artificial range effects are introduced.
- Since our algorithm is based on horizontal echo structure, our results are not strongly dependent on the location of the radar with respect to the precipitation. In contrast, techniques that use the bright band as a major criterion to identify the stratiform precipitation produce results dependent on the location of the radar with respect to the precipitation. Hence, to use the results of such a convective–stratiform separation method as verification, a modeler would have to simulate not only the precipitation (a hard job in itself) but also have to model how the precipitation would look to a radar at a particular location. Our method avoids this difficulty.
- Since the convective–stratiform separation algorithm requires only data collected below the bright band to perform the classification, its use is not restricted to a particular radar scan strategy—that is, times when a full volume scan is collected. Full volume scans, comprising 12 or more tilt-sequence scans arranged so as to provide good coverage from the lowest levels to storm top, are used for tuning the algorithm, but are not necessary to run it. Hence, the algorithm will run equally well with either the 14 or 9 elevation angle NEXRAD precipitation mode scanning strategies (Brandes et al. 1991).

Our algorithm for representing the vertical structure of a set of radar echoes (section 8a) is the CFAD (Yuter and Houze 1995b), which displays the frequency distribution of radar reflectivity values as a function of height. The CFAD summarizes the vertical structure of all the echoes for an entire month (or any other climatological time period) in a single plot. When the data are separated into convective and stratiform subsets, the CFAD shows clearly the narrower distribution and weaker reflectivities of stratiform precipitation and the higher reflectivity and broader distribution associated with convective precipitation.

Once the data have been separated into convective and stratiform components, we may determine the precipitation rates and amounts by any method (e.g., power law or probability matching), as long as the Z–R relation used to convert the reflectivity to rain rate is rain gauge adjusted (sections 10–11). Whether the adjustment is by monthly mean values [e.g., the rain gauge–adjusted power law, Eq. (5), in section 10a] or by percentiles [e.g., the window probability-match-

ing method, section 10c], the monthly rain statistics are affected by less than 10%.

Adjustment to the monthly mean is a more practical method for estimating rain rates and amounts for monthly precipitation climatologies. Probability matching requires a large sample of data to obtain stable estimates of all the percentiles in the frequency distribution of rain rate and reflectivity. To obtain such estimates, a large sample of simultaneous rain rates and reflectivities of various intensities is required. This sampling requirement implies that only high-resolution gauges (e.g., tipping buckets) are useful, and the radar data must be analyzed and compared to the gauges at frequent intervals (every few minutes). Since extreme rain rates occur infrequently, and most operational rain gauges are not high resolution, long records are required (Krajewski and Smith 1991; Rosenfeld et al. 1993). Often the length of record required to achieve a stable statistic of the reflectivity and rain-rate probability distributions is longer than a month. Adjustment to monthly means, on the other hand, requires only a stable estimate of the month's total rain amount from the gauges. All the gauges are used, whether they are high-resolution tipping buckets or simpler accumulation gauges. Thus, more data enter the adjustment, and the required adjustment for monthly statistics is more easily done with data for the month in question. In addition, it is not necessary to analyze the data every few minutes. A simple analysis of a long record of rain gauge data (section 12) shows that sampling precipitation once an hour avoids sampling problems associated with a strong diurnal cycle of precipitation; the uncertainty in the monthly rain accumulation is less than 10%. Sampling the radar data once an hour (the frequency of observation from most accumulation gauges) rather than every 10 min (required by probability matching) is a factor of 6 reduction in the handling of the radar data stream, but still provides a robust basis for monthly Z–R adjustment.

The techniques tested in this paper provide a simple algorithmic approach that will extract physically meaningful information from the digital volumetric radar data and rain gauge network data obtained at operational radar sites. This information will be the basis of climatologies of precipitation structure, amount, and mechanisms. The techniques we propose may be used to verify spaceborne satellite data, such as those to be obtained on the TRMM satellite. However, since our algorithms operate on the data of any operational site with suitable radar and rain gauge instrumentation, they form the basis of a technique for studying precipitation structure on a global basis.

Acknowledgments. We are grateful to Otto Thiele, Dennis Flanigan, and David B. Wolff for providing the Darwin radar and rain gauge data. Thomas D. Keenan provided the sounding data and information regarding the Darwin site. The valuable discussions and comments by Scott Braun and David E. Kingsmill are greatly appreciated. Stacy R. Brodzik, Mark D. Albright, and Michael Steiner provided computational assistance. Shuyi S. Chen contributed Fig. 1 and Kay Dewar assisted with Fig. 13. Grace C. Gudmundson edited the manuscript. This work is supported by NASA Grant NAG 5-1599.

REFERENCES

Andrieu, H., and J. D. Creutin, 1995: Identification of vertical profiles of radar reflectivity for hydrological applications using an inverse method. Part I: Formulation. *J. Appl. Meteor.*, **34,** 225–239.

Atlas, D., D. Rosenfeld, and D. A. Short, 1990a: The estimation of convective rainfall by area integrals. Part I: The theoretical and empirical basis. *J. Geophys. Res.*, **95,** 2153–2160.

——, ——, and D. B. Wolff, 1990b: Climatologically tuned reflectivity–rain rate relations and links to area–time integrals. *J. Appl. Meteor.*, **29,** 1120–1135.

Austin, P. M., 1987: Relation between measured radar reflectivity and surface rainfall. *Mon. Wea. Rev.*, **115,** 1053–1070.

——, and A. C. Bemis, 1950: A quantitative study of the "bright band" in radar precipitation echoes. *J. Meteor.*, **7,** 145–151.

——, S. G. Geotis, J. B. Cunning, J. L. Thomas, R. I. Sax, and J. R. Gillespie, 1976: Raindrop size distributions and Z–R relationship for GATE. *10th Tech. Conf. on Hurricanes and Tropical Meteorology,* Charlottesville, VA, Amer. Meteor. Soc.

Battan, L. J., 1959: *Radar Meteorology.* The University of Chicago Press, 161 pp.

——, 1973: *Radar Observation of the Atmosphere.* The University of Chicago Press, 324 pp.

Bell, T. L., A. Abdullah, R. L. Martin, and G. R. North, 1990: Sampling errors for satellite-derived tropical rainfall: Monte Carlo study using a space–time stochastic model. *J. Geophys. Res.*, **95,** 2195–2205.

Biggerstaff, M. I., and R. A. Houze Jr., 1991: Kinematic and precipitation structure of the 10–11 June 1985 squall line. *Mon. Wea. Rev.*, **119,** 3034–3065.

Brandes, E. A., D. S. Zrnić, G. E. Klazura, C. F. Suprenant, and D. Sirmans, 1991: The Next Generation Weather Radar (WSR-88D) as an applied research tool. Preprints, *25th Int. Conf. on Radar Meteorology,* Paris, France, Amer. Meteor. Soc., 47–50.

Brown, R. C., and V. F. Borgogno, 1980: A laboratory radar display system. Preprints, *19th Conf. on Radar Meteorology,* Miami Beach, FL, Amer. Meteor. Soc., 272–277.

Calheiros, R. V., and I. Zawadzki, 1987: Reflectivity–rain rate relationships for radar hydrology in Brazil. *J. Climate Appl. Meteor.*, **26,** 118–132.

Cheng, C.-P., and R. A. Houze Jr., 1979: The distribution of convective and mesoscale precipitation in GATE radar echo patterns. *Mon. Wea. Rev.*, **107,** 1370–1381.

Cheng, M., and R. Brown, 1993: Estimation of area-average rainfall for frontal rain using the threshold method. *Quart. J. Roy. Meteor. Soc.*, **119,** 825–844.

Chiu, L. S., 1988: Estimating areal rainfall from rain area. *Tropical Rainfall Measurements,* J. S. Theon and N. Fugono, Eds., A. Deepak Publishing, 361–367.

Chong, M., and D. Hauser, 1989: A tropical squall line observed during the COPT 81 experiment in West Africa. Part II: Water budget. *Mon. Wea. Rev.*, **117,** 728–744.

Churchill, D. D., and R. A. Houze Jr., 1984: Development and structure of winter monsoon cloud clusters on 10 December 1978. *J. Atmos. Sci.*, **41,** 933–960.

Collier, C. G., S. Lovejoy, and G. L. Austin, 1980: Analysis of bright bands from 3-D radar data. Preprints, *19th Conf. on Radar Meteorology,* Miami Beach, FL, Amer. Meteor. Soc., 44–47.

Crum, T. D., and R. L. Alberty, 1993: The WSR-88D and the WSR-88D operational support facility. *Bull. Amer. Meteor. Soc.*, **74,** 1669–1687.

——, ——, and D. W. Burgess, 1993: Recording, archiving, and using WSR-88D data. *Bull. Amer. Meteor. Soc.*, **74,** 645–652.

Donaldson, R. J., Jr., 1961: Radar reflectivity profiles in thunderstorms. *J. Meteor.*, **18,** 292–305.

——, 1964: A demonstration of antenna beam errors in radar reflectivity patterns. *J. Appl. Meteor.*, **3,** 611–623.

Doneaud, A. A., P. L. Smith, A. S. Dennis, and S. Sengupta, 1981: A simple method for estimating convective rain volume over an area. *Water Resour. Res.*, **17,** 1676–1682.

——, S. I. Niscov, D. L. Priegnitz, and P. L. Smith, 1984: The area–time integral as an indicator for convective rain volumes. *J. Climate Appl. Meteor.*, **23,** 555–561.

Drosdowsky, W., 1984: Structure of a northern Australian squall line system. *Aust. Meteor. Mag.*, **32,** 177–183.

Dye, J. E., B. E. Martner, and J. E. Miller, 1983: Dynamical–microphysical evolution of a convective storm in a weakly sheared environment. Part I: Microphysical observations and interpretation. *J. Atmos. Sci.*, **40,** 2083–2096.

Fabry, F., G. L. Austin, and D. Tees, 1992: The accuracy of rainfall estimates by radar as a function of range. *Quart. J. Roy. Meteor. Soc.*, **118,** 435–453.

——, A. Bellon, and I. Zawadzki, 1994: Long term observations of the melting layer using vertically pointing radars. Research Report of the Cooperative Centre for Research in Mesometeorology (formerly Stormy Weather Group), MW-101, McGill University, Montreal, Quebec, Canada, 65 pp.

Gage, K. S., C. R. Williams, and W. L. Ecklund, 1994: UHF wind profilers: A new tool for diagnosing tropical convective cloud systems. *Bull. Amer. Meteor. Soc.*, **75,** 2289–2294.

Gamache, J. F., and R. A. Houze Jr., 1982: Mesoscale air motions associated with a tropical squall line. *Mon. Wea. Rev.*, **110,** 118–135.

——, and ——, 1983: Water budget of a mesoscale convective system in the tropics. *J. Atmos. Sci.*, **40,** 1835–1850.

Gupta, V. K., and E. Waymire, 1990: Multiscaling properties of spatial rainfall and river flow distributions. *J. Geophys. Res.*, **95,** 1999–2009.

Heymsfield, A. J., and D. J. Musil, 1982: Case study of a hailstorm in Colorado. Part II: Particle growth processes at midlevels deduced from in-situ measurements. *J. Atmos. Sci.*, **39,** 2847–2866.

Hobbs, P. V., 1973: Ice in the atmosphere: A review of the present position. *Physics and Chemistry of Ice,* E. Whalley, S. J. Jones, and L. W. Gold, Eds., Royal Society of Canada, 308–319.

Holland, G. J., 1986: Interannual variability of the Australian summer monsoon at Darwin: 1952–82. *Mon. Wea. Rev.*, **114,** 594–604.

Houghton, H. G., 1968: On precipitation mechanisms and their artificial modification. *J. Appl. Meteor.*, **7,** 851–859.

Houze, R. A., Jr., 1973: A climatological study of vertical transports by cumulus-scale convection. *J. Atmos. Sci.*, **30,** 1112–1123.

——, 1977: Structure and dynamics of a tropical squall-line system. *Mon. Wea. Rev.*, **105,** 1540–1567.

——, 1982: Cloud clusters and large-scale vertical motions in the tropics. *J. Meteor. Soc. Japan,* **60,** 396–410.

——, 1989: Observed structure of mesoscale convective systems and implications for large-scale heating. *Quart. J. Roy. Meteor. Soc.*, **115,** 425–461.

——, 1993: *Cloud Dynamics.* Academic Press, 573 pp.

——, and C.-P. Cheng, 1977: Radar characteristics of tropical convection observed during GATE: Mean properties and trends over the summer season. *Mon. Wea. Rev.*, **105,** 964–980.

——, and A. K. Betts, 1981: Convection in GATE. *Rev. Geophys. Space Phys.*, **19,** 541–576.

——, and D. D. Churchill, 1984: Microphysical structure of winter monsoon cloud clusters. *J. Atmos. Sci.*, **41,** 3405–3411.

——, and E. N. Rappaport, 1984: Air motions and precipitation structure of an early summer squall line over the eastern tropical Atlantic. *J. Atmos. Sci.*, **41,** 553–574.

——, and D. D. Churchill, 1987: Mesoscale organization and cloud microphysics in a Bay of Bengal depression. *J. Atmos. Sci.*, **44,** 1845–1867.

——, P. V. Hobbs, K. R. Biswas, and W. M. Davis, 1976: Mesoscale rainbands in extratropical cyclones. *Mon. Wea. Rev.*, **105,** 868–878.

——, B. F. Smull, and P. Dodge, 1990: Mesoscale organization of springtime rainstorms in Oklahoma. *Mon. Wea. Rev.*, **117,** 613–654.

Hudlow, M., 1979: Mean rainfall patterns for the three phases of GATE. *J. Appl. Meteor.*, **18,** 1656–1669.

Huschke, R. E., Ed., 1959: *Glossary of Meteorology.* Amer. Meteor. Soc., 638 pp.

Johnson, R. H., 1984: Partitioning tropical heat and moisture budgets into cumulus and mesoscale components: Implications for cumulus parameterization. *Mon. Wea. Rev.*, **112,** 1590–1601.

——, and R. A. Houze Jr., 1987: Precipitating cloud systems of the Asian monsoon. *Monsoon Meteorology,* C. P. Chang and T. N. Krishnamurti, Eds., Oxford University Press, 298–353.

——, and P. J. Hamilton, 1988: The relationship of surface pressure features to the precipitation and airflow structure of an intense midlatitude squall line. *Mon. Wea. Rev.*, **116,** 1444–1472.

Joss, J., and A. Waldvogel, 1970: A method to improve the accuracy of radar-measured amounts of precipitation. Preprints, *14th Radar Meteorology Conf.*, Tucson, AZ, Amer. Meteor. Soc., 237–238.

——, and ——, 1990: Precipitation measurements and hydrology. *Radar in Meteorology,* D. Atlas, Ed., Amer. Meteor. Soc., 577–606.

——, J. C. Thams, and A. Waldvogel, 1968: The accuracy of daily rainfall measurements by radar. *Proc. 13th Radar Meteorology Conf.*, Montreal, Canada, Amer. Meteor. Soc., 448–451.

——, K. Schram, J. C. Thams, and A. Waldvogel, 1970: On the quantitative determination of precipitation by radar. Wiss. Mitteilung Nr. 63 der Eidgen. Kommission zum Studium der Hagelbildung und der Hagelabwehr, Swiss Federal Institute of Technology (ETH), Zurich, Switzerland, 38 pp.

Kedem, B., L. S. Chiu, and Z. Karni, 1990: An analysis of the threshold method for measuring area-average rainfall. *J. Appl. Meteor.*, **29,** 3–20.

Keenan, T. D., and R. E. Carbone, 1992: A preliminary morphology of precipitation systems in tropical northern Australia. *Quart. J. Roy. Meteor. Soc.*, **118,** 283–326.

——, G. J. Holland, M. J. Manton, and J. Simpson, 1988: TRMM ground truth in a monsoon environment: Darwin, Australia. *Aust. Meteor. Mag.*, **36,** 81–90.

——, B. R. Morton, M. J. Manton, and G. J. Holland, 1989: The Island Thunderstorm Experiment (ITEX)—A study of tropical thunderstorms in the maritime continent. *Bull. Amer. Meteor. Soc.*, **70,** 152–159.

——, ——, X. S. Zhang, and K. Nyguen, 1990: Some characteristics of thunderstorms over Bathurst and Melville Islands near Darwin, Australia. *Quart. J. Roy. Meteor. Soc.*, **116,** 1153–1172.

Kitchen, M., and P. M. Jackson, 1993: Weather radar performance at long range—Simulated and observed. *J. Appl. Meteor.*, **32,** 975–985.

Klazura, G. E., 1981: Differences between some radar-rainfall estimation procedures in a high rain rate gradient storm. *J. Appl. Meteor.*, **20,** 1376–1380.

Knight, C. A., W. A. Cooper, D. W. Breed, I. R. Paluch, R. L. Smith, and G. Vali, 1982: Microphysics. Vol. 1, *Hailstorms of the Central High Plains,* C. A. Knight and P. Squires, Eds., Colorado Associated University Press, 151–191.

Krajewski, W. F., and J. A. Smith, 1991: On the estimation of climatological Z–R relationships. *J. Appl. Meteor.*, **30,** 1436–1445.

——, M. L. Morrissey, J. A. Smith, and D. T. Rexroth, 1992: The accuracy of the area-threshold method: A model-based simulation study. *J. Appl. Meteor.*, **31,** 1396–1406.

Leary, C. A., 1984: Precipitation structure of the cloud clusters in a tropical easterly wave. *Mon. Wea. Rev.*, **112,** 313–325.

López, R. E., 1976: Radar characteristics of the cloud populations of tropical disturbances in the northwest Atlantic. *Mon. Wea. Rev.*, **104,** 268–283.

——, D. Atlas, D. Rosenfeld, J. L. Thomas, D. O. Blanchard, and R. L. Holle, 1989: Estimation of areal rainfall using the radar echo area time integral. *J. Appl. Meteor.*, **28,** 1162–1175.

Lovejoy, S., and D. Schertzer, 1990: Multifractals, universality classes and satellite and radar measurements of cloud and rain fields. *J. Geophys. Res.*, **95,** 2021–2034.

Mapes, B. E., and R. A. Houze Jr., 1992: An integrated view of the 1987 Australian monsoon and its mesoscale convective systems. Part I: Horizontal structure. *Quart. J. Roy. Meteor. Soc.*, **118,** 927–963.

——, and ——, 1993: An integrated view of the 1987 Australian monsoon and its mesoscale convective systems. Part II: Vertical structure. *Quart. J. Roy. Meteor. Soc.*, **119,** 733–754.

Matejka, T. J., R. A. Houze Jr., and P. V. Hobbs, 1980: Microphysics and dynamics of clouds associated with mesoscale rainbands in extratropical cyclones. *Quart. J. Roy. Meteor. Soc.*, **106,** 29–56.

Matsuo, T., and Y. Sasyo, 1981: Melting of snowflakes below freezing levels in the atmosphere. *J. Meteor. Soc. Japan,* **59,** 10–25.

Miller, J. R., 1972: A climatological Z–R relationship for convective storms in the northern Great Plains. Preprints, *15th Radar Meteorology Conf.,* Champaign–Urbana, IL, Amer. Meteor. Soc., 153–154.

Mohr, C. G., and R. L. Vaughan, 1979: An economical procedure for Cartesian interpolation and display of reflectivity factor data in three-dimensional space. *J. Appl. Meteor.*, **18,** 661–670.

Oye, R., and R. Carbone, 1981: Interactive Doppler editing software. Preprints, *20th Conf. on Radar Meteorology,* Boston, MA, Amer. Meteor. Soc., 683–689.

Ramage, C. S., 1968: Role of a tropical "maritime continent" in the atmospheric circulation. *Mon. Wea. Rev.*, **96,** 365–370.

Rinehart, R. E., 1991: *Radar for Meteorologists.* 2d ed. University of North Dakota, 334 pp. [Available from the Department of Atmospheric Sciences, University of North Dakota, Grand Forks, ND 58202-8216.]

Rogers, R. R., 1979: *A Short Course in Cloud Physics.* 2d ed. Pergamon Press, 235 pp.

Rosenfeld, D., D. Atlas, and D. A. Short, 1990: The estimation of rainfall by area integrals. Part II: The height–area rainfall threshold (HART) method. *J. Geophys. Res.*, **95,** 2161–2176.

——, D. Atlas, D. B. Wolff, and E. Amitai, 1992: Beamwidth effects on Z–R relations and area-integrated rainfall. *J. Appl. Meteor.*, **31,** 454–464.

——, D. B. Wolff, and D. Atlas, 1993: General probability-matched relations between radar reflectivity and rain rate. *J. Appl. Meteor.*, **32,** 50–72.

——, ——, and E. Amitai, 1994: The window probability matching method for rainfall measurements with radar. *J. Appl. Meteor.*, **33,** 682–693.

——, E. Amitai, and D. B. Wolff, 1995: Classification of rain regimes by the three-dimensional properties of reflectivity fields. *J. Appl. Meteor.*, **34,** 198–211.

Rutledge, S. A., and D. R. McGorman, 1988: Cloud-to-ground lightning activity in the 10–11 June 1985 convective system observed during the Oklahoma–Kansas PRE-STORM project. *Mon. Wea. Rev.*, **116,** 1393–1408.

Ryde, J. W., 1946: The attenuation and radar echoes produced at centimeter wavelengths by various meteorological phenomena. *Meteorological Factors in Radio Wave Propagation,* Physical Society, London, 169–188.

Seed, A., and G. L. Austin, 1990: Variability of summer Florida rainfall and its significance for the estimation of rainfall by gages, radar, and satellite. *J. Geophys. Res.*, **95,** 2207–2215.

Short, D. A., T. Kozu, and K. Nakamura, 1990: Rainrate and raindrop size distribution observations in Darwin Australia. *Proc., URSI Commission F Open Symp. on Regional Factors in Predicting Radiowave Attenuation due to Rain,* Rio de Janeiro, Brazil, URSI, 35–40.

——, D. B. Wolff, D. Rosenfeld, and D. Atlas, 1993: A study of the threshold method utilizing raingauge data. *J. Appl. Meteor.*, **32,** 1379–1387.

Simpson, J., Ed., 1988: TRMM: A satellite mission to measure tropical rainfall, report of the science steering group. National Aeronautics and Space Administration, Goddard Space Flight Center, 94 pp. [Available from NASA/GSFC, Greenbelt, MD 20771.]

——, R. F. Adler, and G. R. North, 1988: A proposed Tropical Rainfall Measuring Mission (TRMM) satellite. *Bull. Amer. Meteor. Soc.*, **69,** 278–295.

——, T. D. Keenan, B. Ferrier, R. H. Simpson, and G. J. Holland, 1993: Cumulus mergers in the maritime continent region. *Meteor. Atmos. Phys.*, **51,** 73–99.

Smith, J. A., 1993: Marked point process models of raindrop-size distributions. *J. Appl. Meteor.*, **32,** 284–296.

——, and W. F. Krajewski, 1987: Statistical modeling of space–time rainfall using radar and raingauge observations. *Water Resour. Res.*, **23,** 1893–1900.

——, and ——, 1993: A modeling study of rainfall rate-reflectivity relationships. *Water Resour. Res.*, **29,** 2505–2514.

Smith, P. L., 1990: Precipitation measurements and hydrology: Panel report. *Radar in Meteorology,* D. Atlas, Ed., Amer. Meteor. Soc., 607–618.

Steiner, M., and A. Waldvogel, 1989: The bright band and its influence on microphysics. Preprints, *24th Conf. on Radar Meteorology,* Tallahassee, FL, Amer. Meteor. Soc., 5–8.

——, and R. A. Houze Jr., 1993: Three-dimensional validation at TRMM ground truth sites: Some early results from Darwin, Australia. Preprints, *26th Int. Conf. on Radar Meteorology,* Norman, OK, Amer. Meteor. Soc., 417–420.

Tao, W.-K., S. Lang, J. Simpson, and R. Adler, 1993: Retrieval algorithms for estimating the vertical profiles of latent heat release: Their applications for TRMM. *J. Meteor. Soc. Japan,* **71,** 685–700.

Thiele, O. W., 1988: Validating space observations of rainfall. *Tropical Rainfall Measurements,* J. S. Theon and N. Fugono, Eds., A. Deepak Publishing, 415–423.

——, D. B. Wolff, D. A. Makofski, and B. Fisher, 1992: Tropical Rainfall Measuring Mission (TRMM), data catalog. National Aeronautics and Space Administration, Goddard Space Flight Center, 82 pp. [Available from NASA/GSFC, Greenbelt, MD 20771.]

Waldvogel, A., L. Klein, D. J. Musil, and P. L. Smith, 1987: Characteristics of radar-identified big drop zones in Swiss hailstorms. *J. Climate Appl. Meteor.*, **26,** 861–877.

Wei, T., and R. A. Houze Jr., 1987: The GATE squall line of 9–10 August 1974. *Adv. Atmos. Sci.*, **4,** 85–92.

Wexler, R., and D. Atlas, 1956: Factors influencing radar echo intensities in the melting layer. *Quart. J. Roy. Meteor. Soc.*, **82,** 349–351.

Wilson, J. W., and E. A. Brandes, 1979: Radar measurement of rainfall—A summary. *Bull. Amer. Meteor. Soc.*, **60,** 1048–1058.

Yuter, S. E., and R. A. Houze Jr., 1995a: Three-dimensional kinematic and microphysical evolution of Florida cumulonimbus. Part I: Spatial distribution of updrafts, downdrafts, and precipitation. *Mon. Wea. Rev.*, **123,** 1921–1940.

——, and ——, 1995b: Three-dimensional kinematic and microphysical evolution of Florida cumulonimbus. Part II: Frequency distributions of vertical velocity, reflectivity and differential reflectivity. *Mon. Wea. Rev.*, **123,** 1941–1963.

——, and ——, 1995c: Three-dimensional kinematic and microphysical evolution of Florida cumulonimbus. Part III: Vertical mass transport, mass divergence and synthesis. *Mon. Wea. Rev.*, **123,** 1964–1983.

Zawadzki, I., 1984: Factors affecting the precision of radar measurements of rain. Preprints, *22d Conf. on Radar Meteorology,* Zurich, Switzerland, Amer. Meteor. Soc., 251–256.

Zipser, E. J., and K. R. Lutz, 1994: The vertical profile of radar reflectivity of convective cells: A strong indicator of storm intensity and lightning probability. *Mon. Wea. Rev.*, **122,** 1751–1759.